



MADS1 maintains barley spike morphology at high ambient temperatures

Gang Li^{1,2}✉, Hendrik N. J. Kuijer¹, Xiujuan Yang¹, Huiran Liu³, Chaoqun Shen^{1,3}, Jin Shi³, Natalie Betts¹, Matthew R. Tucker¹, Wanqi Liang^{1,3}, Robbie Waugh^{1,4,5}, Rachel A. Burton¹ and Dabing Zhang^{1,3}✉

Temperature stresses affect plant phenotypic diversity. The developmental stability of the inflorescence, required for reproductive success, is tightly regulated by the interplay of genetic and environmental factors. However, the mechanisms underpinning how plant inflorescence architecture responds to temperature are largely unknown. We demonstrate that the barley SEPALLATA MADS-box protein HvMADS1 is responsible for maintaining an unbranched spike architecture at high temperatures, while the loss-of-function mutant forms a branched inflorescence-like structure. HvMADS1 exhibits increased binding to target promoters via A-tract CArG-box motifs, which change conformation with temperature. Target genes for high-temperature-dependent HvMADS1 activation are predominantly associated with inflorescence differentiation and phytohormone signalling. HvMADS1 directly regulates the cytokinin-degrading enzyme HvCKX3 to integrate temperature response and cytokinin homeostasis, which is required to repress meristem cell cycle/division. Our findings reveal a mechanism by which genetic factors direct plant thermomorphogenesis, extending the recognized role of plant MADS-box proteins in floral development.

As sessile organisms, plants have undergone long-term phenological and morphological adaptations to elevated temperatures^{1–3}. These adaptive mechanisms respond to gradual increases in temperature by modifying a suite of developmental traits, such as flowering time, stem elongation and seed germination^{4,5}. In *Arabidopsis thaliana*, several key sensors/regulators have been reported to be involved in thermal adaptation. Histone variant H2A.Z contributes to chromatin remodelling in response to temperature changes⁶, and both PHYTOCHROMES (PHYs) and the basic helix-loop-helix transcription factor PHYTOCHROME INTERACTING FACTOR4 (PIF4) function in temperature regulatory responses and thermomorphogenesis that lead to developmental and architectural variations^{7,8}. However, the factors that establish and maintain phenology and organ identity in response to temperature changes remain unknown.

Plant inflorescence morphology is determined by the arrangement of the plant's branches and florets, developmental processes that are governed by a range of genetic and environmental factors^{3,9–12}. Fitness landscape model predictions of inflorescence architecture and the Watson and Dallwitz database of flowering plants reveal higher frequencies of cyme plants (flowers terminating the axis) in temperate than in tropical climes, possibly because there is a benefit associated with the sequential maturity of flowers in cymes, and the opposite for highly branched panicles¹². Plants with unbranched raceme-type inflorescences are also shown to be more frequent in temperate than in tropical conditions, but not significantly¹², suggesting a complex interaction between inflorescence development and environmental adaptation. Triticeae crops, such as wheat (*Triticum* spp.) and barley (*Hordeum vulgare*), have unbranched inflorescences (spikes) where the flower-producing

spikelets are attached directly to the main axis of the inflorescence. An increase in ambient temperature (for example, >25 °C) leads to delayed inflorescence meristem development and reduces the number of spikelet primordia in both wheat and barley¹³, indicating that high temperatures inhibit both inflorescence and spikelet development during early reproductive stages of Triticeae crops. With climate change likely to drive changes in global plant phenology^{2,14}, the adaptation of fitness-related traits is becoming paramount in plants, including many crops^{1,2,13,15}. Extreme temperature changes are speculated to impact reproductive growth in particular¹⁶, which is potentially devastating for grain yield in cereal crops^{17,18}. However, the mechanisms by which plants alter inflorescence structure under changing environmental temperatures are poorly understood.

SEPALLATA (SEP) proteins are plant E-class MADS-box family transcription factors that regulate a wide variety of reproductive events, including flowering time, inflorescence architecture, flower organ development and fruit ripening^{19–23}. Like other MADS-box proteins, SEPs bind a canonical CArG-box DNA motif (CC(A/T)_nGG or C(A/T)_nG) to regulate target gene expression^{24,25}. Strikingly, the curvature of DNA regions containing A-tract elements that minimize the incidence of TpA sites in the (A/T)_n core strongly depends on temperature, which may affect in vivo binding by transcription factors^{25–28}. However, whether or how MADS-box proteins regulate in vivo thermal gene expression and plant thermomorphogenesis remains unknown.

Here, we examine the role of SEPs in directing inflorescence architecture in barley. Our results demonstrate that one SEP, HvMADS1, is critical in maintaining an unbranched barley spike under high ambient temperatures by modulating cytokinin (CK) homeostasis, providing insights into inflorescence thermomorphogenesis.

¹School of Agriculture, Food and Wine, Waite Research Institute, The University of Adelaide, Waite Campus, Glen Osmond, South Australia, Australia.

²School of Life Sciences and Engineering, Southwest University of Science and Technology, Mianyang, China. ³Joint International Research Laboratory of Metabolic and Developmental Sciences, Shanghai Jiao Tong University–University of Adelaide Joint Centre for Agriculture and Health, State Key Laboratory of Hybrid Rice, School of Life Sciences and Biotechnology, Shanghai Jiao Tong University, Shanghai, China. ⁴James Hutton Institute, Dundee, UK. ⁵Division of Plant Sciences, School of Life Sciences, University of Dundee, Dundee, UK. ✉e-mail: gang.li@adelaide.edu.au; dabing.zhang@adelaide.edu.au

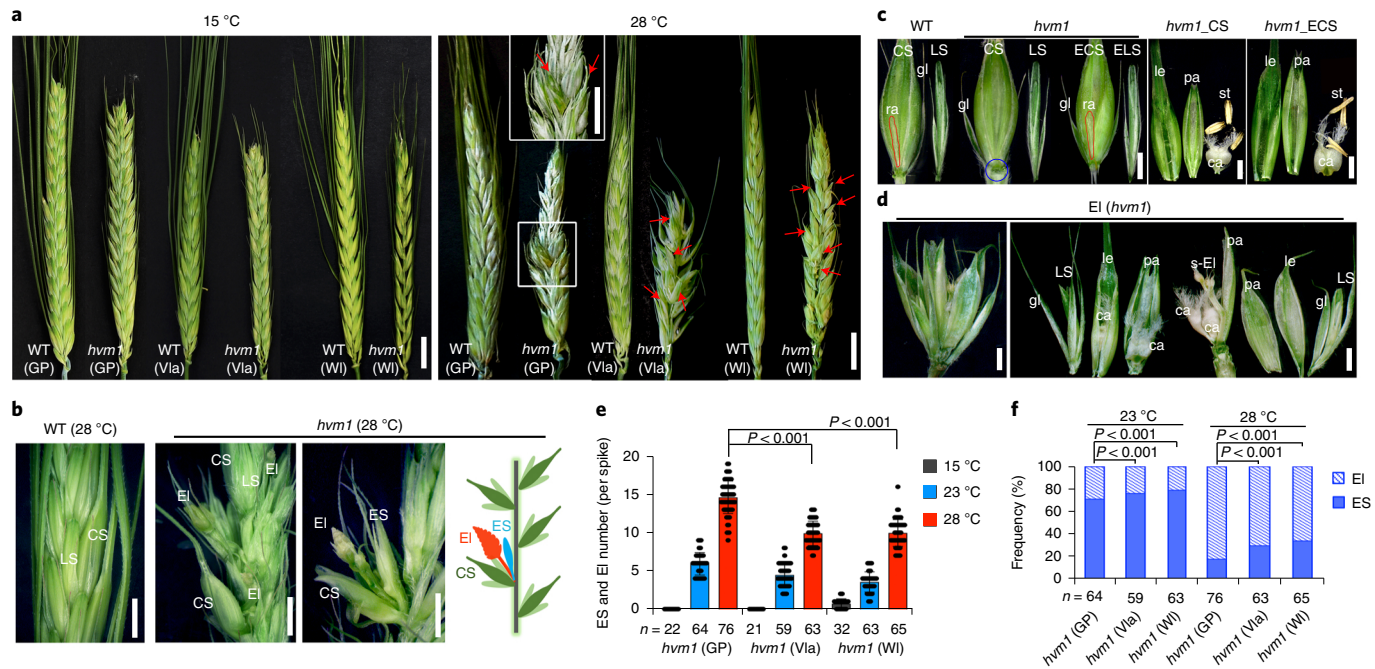


Fig. 1 | HvMADS1 regulates inflorescence plasticity in response to high temperature. **a**, Inflorescence phenotypes of wild-type (WT) plants and *Hvmads1* (*hvm1*) mutants in GP, Vla and WI backgrounds, under control (15 °C day/10 °C night) and heat stress (28 °C day/23 °C night) conditions. The red arrows indicate the ectopic organs. Scale bars, 1 cm. **b**, High-temperature conditions induce the formation of ESs and EIs in *hvm1* but not in WT (GP) spikes. CS, central spikelet; LS, lateral spikelet. Scale bars, 1 cm. The schematic of *hvm1* inflorescence architecture shows an ES (blue) and an EI (red). **c**, Morphology of a CS and an LS in WT and *hvm1*, and a CS and an LS from ectopic spikelets (ECS and ELS) in *hvm1* at 28 °C. gl, glume; ra, rachilla (red boundary); le, lemma; pa, palea; st, stamen; ca, carpel. The blue circle indicates the initiated position of ESs and EIs. Scale bars, 0.2 cm. **d**, Phenotype of an EI and its floret organ from *hvm1* at 28 °C. s-EI, secondary EI branch. Scale bars, 0.2 cm. **e**, The average number of ectopic organs (ESs and EIs) per spike in *hvm1* mutants (three genotypic backgrounds) at three temperatures. The data are shown as mean \pm s.d. The *P* values indicate the results from pairwise comparisons of one-way analysis of variance (ANOVA) tests. **f**, The proportion of EIs:ESs produced in response to high ambient temperatures. The *P* values indicate the results from pairwise comparisons of two-way ANOVA tests. All experiments with treatments were repeated four times, with similar results.

Results

HvMADS1 regulates inflorescence plasticity in response to high temperature. In barley, there are five *SEP* genes in two clades: one *LOFSEP* clade with three members (*HvMADS1*, *HvMADS5* and *HvMADS34*) and the other clade with two *SEP3*-like genes (*HvMADS7* and *HvMADS8*) (ref. ²⁹). These five genes are known to be highly expressed in developing inflorescences on the basis of our previous RNA-seq data³⁰. *LOFSEP*-like family members and their orthologues are associated with inflorescence architecture regulation in *Arabidopsis*²¹, rice (*Oryza sativa*)²² and tomato (*Solanum lycopersicum*)²³. To explore the genetic basis of barley inflorescence development, we used CRISPR-Cas9 (ref. ³¹) in the UK barley variety Golden Promise (GP) to create individual loss-of-function mutants and double mutants of three *LOFSEP* MADS-box genes: *HvMADS1*, *HvMADS5* and *HvMADS34* (Extended Data Fig. 1a–e). Under control growing conditions (15 °C day/10 °C night), none of the mutants displayed any visible changes in spike architecture or organ morphology in either the central or lateral spikelets, except that spikes of *Hvmads1* single and double (*Hvmads1/5* and *Hvmads1/34*) mutants produced shorter awns than wild-type plants (Fig. 1a and Extended Data Figs. 2 and 3). Under heat stress conditions (28 °C day/23 °C night), spikes of *Hvmads1* single and double mutants produced ectopic spike/spikelet-like organs, while *Hvmads5*, *Hvmads34* and *Hvmads5/34* mutants exhibited wild-type spike architecture (Fig. 1a,b and Extended Data Fig. 2), indicating that *HvMADS1* acts a key regulator involved in directing spike architecture in response to temperature. Detailed phenotypic analysis revealed that the heat-induced ectopic organs in *Hvmads1* spikes emerged from the base of the central spikelet,

attached to the joint between the central spikelet and main spike axis (rachis) (Fig. 1b and Extended Data Fig. 4a–c). Some young branch-like meristems were formed at late stages of main spike development, suggesting that high temperature continually induced the initiation of ectopic organs in the mutant (Extended Data Fig. 4b). Morphologically, these new organs could be classified as ectopic inflorescence-like structures (EIs) or ectopic spikelet-like structures (ESs) (Fig. 1b and Extended Data Fig. 4d–f), which emerged more often at the basal end of the main spike (Extended Data Fig. 4g). More EIs and ESs developed with increasing temperature, with *Hvmads1* spikes producing twice as many spikelets (including ectopic spikelets and meristems from EIs or ESs) as wild-type spikes at 28 °C (Extended Data Fig. 4h,i). Compared with the wild type, the central spikelet of the *Hvmads1* mutants at 28 °C lost the rachilla (a secondary rachis at the germ end of the ventral crease of the barley spikelet) but developed normal glumes, lemmas, paleas and lateral spikelets (Fig. 1c), suggesting that some EIs or ESs are probably reverted from the rachilla of the central spikelet. Reversion of the rachilla has also been reported in other barley branched inflorescence mutants, such as *Hvcom1* (*compositum 1*), *Hvcom2* and *Hvvrs4* (*six-rowed spike 4*)^{32–34}. The *Hvmads1* ESs produced at 28 °C showed a normal flower organ structure (Fig. 1c), but the *Hvmads1* EIs exhibited defective flower morphology with multiple lemmas, paleas or carpels in spike-like structures. Occasional secondary EIs with a long, rachis-like axis were observed within these defective spikelets (Fig. 1d).

To confirm that the phenotype is associated with high temperature, we created *Hvmads1* mutants in two Australian barley varieties, Vlamingh (Vla, Western Australia) and WI4330 (WI, South

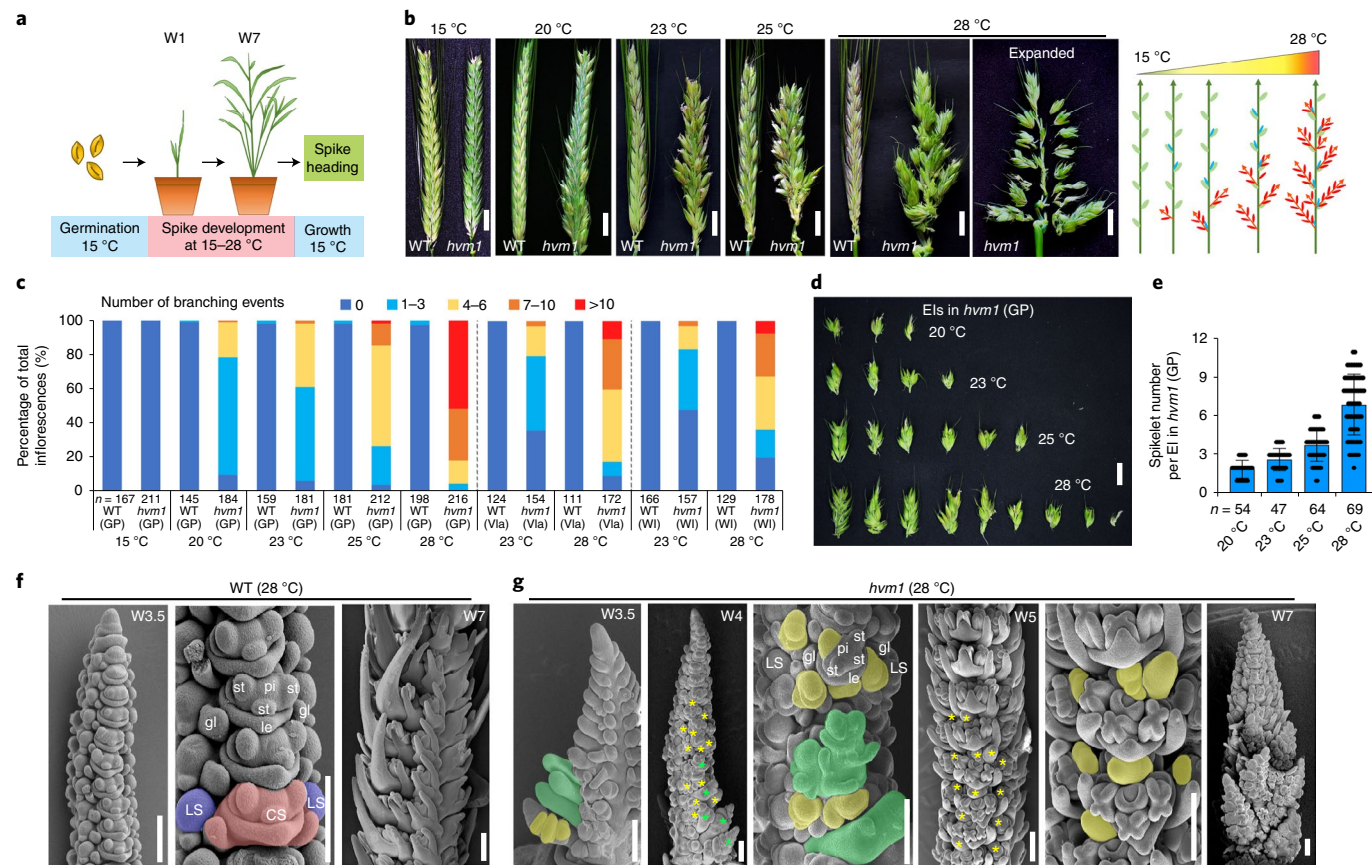


Fig. 2 | High ambient temperatures induce branching events in *Hvmads1*. **a**, Temperature treatment programmes. W1 and W7 indicate Waddington stages of spike development³⁵. **b**, Dosage-dependent high ambient temperatures induce ectopic organs (ESs and EIs) in *hvm1* spikes but not in WT (GP) spikes. Scale bars, 1cm. The schematic of *hvm1* inflorescence architecture indicates ESs in blue and EIs in red. **c**, Quantification of branching events in *hvm1* spikes (three genetic backgrounds) at high-temperature conditions. **d**, El branches of *hvm1* (GP) at high temperatures. Scale bar, 1cm. **e**, Average spikelet number per El at higher temperatures. The data are shown as mean \pm s.d. **f,g**, Scanning electron microscopy of WT (GP) (**f**) and *hvm1 (**g**) spike morphology at 28 °C. pi, pistil. The pink shading indicates a CS, the blue shading indicates LSs, the green shading and green asterisks indicate the indeterminate inflorescence meristem (possibly converted from the CSMs), and the yellow shading and yellow asterisks indicate the ectopic initiated meristems or inflorescence/spikelet meristems (which may be reverted from rachillas). El/ES meristems are shown. Scale bars, 200 μ m. All experiments were repeated three times independently, with similar phenotypes.*

Australia), adapted to a warmer climate than GP (Extended Data Fig. 1a–c). The *Hvmads1*/Vla and *Hvmads1*/WI spikes also produced shorter awns at control temperatures (Fig. 1a and Extended Data Fig. 3a,b) and grew new ectopic organs at high temperatures (Fig. 1a and Extended Data Fig. 4j,k), although less frequently than *Hvmads1* spikes in the GP background (Fig. 1e,f). As growth temperature increased, the number of EIs and ESs also increased (Fig. 1e and Extended Data Fig. 4h), as did the proportion of EIs compared with ESs in all three backgrounds (Fig. 1f). Taken together, our observations indicate that HvMADS1 regulates barley inflorescence architecture in response to temperature.

High ambient temperatures induce branching events in *Hvmads1*. To further assess the role of HvMADS1 in temperature-associated spike meristem development, wild-type (GP) and mutant plants were grown at five different temperatures, including control (15 °C), high ambient (20 °C, 23 °C and 25 °C), and heat stress (28 °C) conditions, from Waddington stage W1 (initiation of inflorescence meristem) to W7 (completion of spike morphogenesis)³⁵ (Fig. 2a). Overall, more ectopic organs and branch-like structures were produced as the temperature increased (Fig. 2b–d), indicating a dosage-dependent, rather than threshold, effect of temperature on *Hvmads1* phenotypes. Similar to the phenotype of *Hvmads1* in a

GP background, more branching events were observed in *Hvmads1* inflorescences in Vla and WI backgrounds at 28 °C than at 23 °C (Fig. 2c).

After high-temperature treatments, plants were transferred back into control temperature conditions (15 °C). EIs further developed into two types: short EIs with a few spikelets and elongated EIs producing normal spikelet-like structures (Fig. 2d,e and Extended Data Fig. 4l,m). Most of the spikelets from short EIs had abnormal organs, including extra glumes, lemmas, paleas, carpels and secondary EIs (Fig. 1d and Extended Data Fig. 4l). We observed a higher proportion of short EIs at lower temperatures (20 °C, up to 90%) than at 28 °C (decreased to ~60%). Elongated EIs showed the converse trend (Extended Data Fig. 4n). While central spikelets from ESs and EIs could produce grains at all elevated temperatures, the overall fertility of ESs and EIs decreased as temperature increased (Extended Data Fig. 4o–q). This indicates that the ectopic spikelets have normal seed-setting capacity that is impacted by temperature.

Scanning electron microscopy revealed no morphological difference between wild-type (GP) and *Hvmads1* inflorescence development at 15 °C, other than retarded awn elongation in the mutant (Extended Data Fig. 5a,b). At 28 °C, *Hvmads1* spikes showed three types of changes to meristem identity: determinate central spikelet meristems (CSMs) probably converted into indeterminate

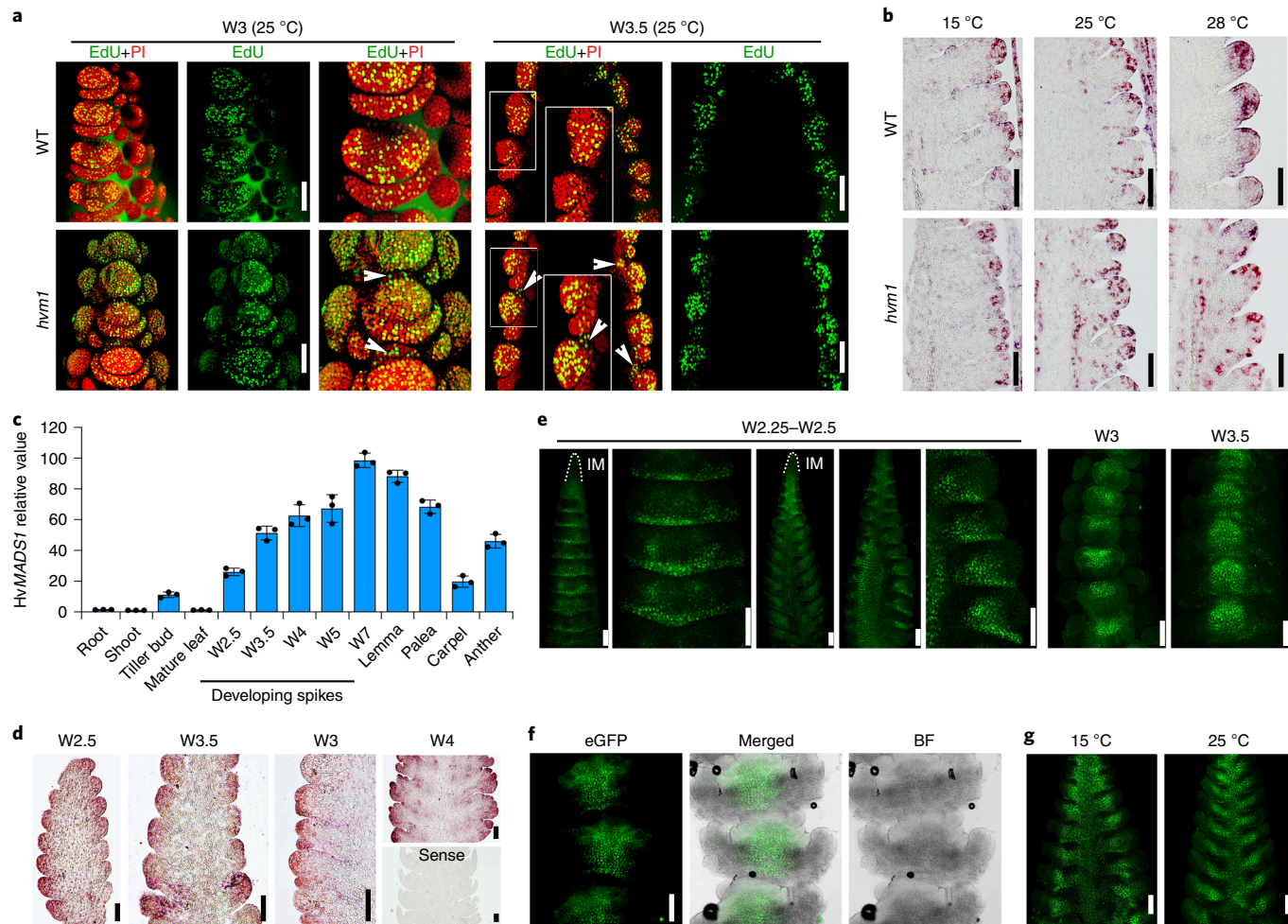


Fig. 3 | HvMADS1 represses ectopic cell division activity of meristems at high temperature. **a**, Cell division activity in WT and *hvm1* spikes at W3 and W3.5 at 25 °C. EdU is indicated by the green signals; propidium iodide (PI) is indicated by the red signals. The white arrowheads indicate high levels of cell division activity in ES/EI meristems. Scale bars, 100 µm. **b**, In situ hybridization showing the expression of the cell division gene, *HvHistone4*, in WT and *hvm1* spikes at 15 °C, 25 °C and 28 °C. Scale bars, 100 µm. **c**, Relative HvMADS1 mRNA levels (RT-qPCR) in different organs and stages of spike development in the WT (GP) compared with control genes *HvActin7* and *HvEF2*. The data are shown as mean ± s.d.; $n=3$ biological replicates. **d**, In situ hybridization of HvMADS1 in longitudinal sections of developing WT spikes at stages W2.5–W4. The sense probe served as a negative control. Scale bars, 100 µm. **e,f**, Accumulation of the HvMADS1 protein in spikes from W2.25 (triple mound stage) to W3.5 (**e**) and a developing spikelet at W5 (**f**) in *pro::HvMADS1-eGFP* transgenic lines at 15 °C. IM, inflorescence meristem; BF, bright field. Scale bars, 100 µm. **g**, Accumulation of HvMADS1 protein in W3.5 *pro::HvMADS1-eGFP* transgenic spikes grown at 15 °C and 25 °C. Scale bars, 100 µm. The experiments in **a–d** were repeated three times independently, with similar results. At least 15 samples of each stage in **e–g** from four independent replicates were observed, with similar results.

inflorescence meristems, the rachilla meristem possibly converted into spikelet/inflorescence-like meristems, and ectopic meristems were newly initiated (Fig. 2f,g and Extended Data Fig. 5c,d). Some CSMs at the base of the main spike appeared to be transformed into inflorescence meristems, which were frequently seen at early stages of spike development (W2.5–W4.0), indicating that the lost determinacy of CSMs may lead to the initiation of branch meristems in the *Hvmads1* mutant under high temperatures. Spikelet/inflorescence-like meristems possibly reverted from rachilla meristems were observed from W2.5. However, the appearance of ectopic meristems was more frequently seen in the middle section of spike later in development (W5), even though the main central spikelets were completely formed (Fig. 2g and Extended Data Fig. 5d), suggesting that the lost determinacy of CSMs may lead to the delayed initiation and development of extra meristems. These data are consistent with our observations that ectopic organs are continually induced under high temperatures (Extended Data Fig. 4b). Thus, inflorescence meristems that were possibly reverted from

rachillas or CSMs and the ectopic meristems around CSMs all probably contribute to the branching phenotype of *Hvmads1* spikes under high temperatures.

Heat stress conditions led to reduced meristem determinacy and the production of ectopic meristems that developed into ESs or EIs. Similar developmental defects were observed in *Hvmads1* mutants at intermediately high ambient temperatures (20–25 °C) (Extended Data Fig. 5e). Moreover, we observed that in all three backgrounds of barley varieties, the *Hvmads1* mutation delayed inflorescence development, including spikelet meristem formation and differentiation, compared with the wild type (Extended Data Fig. 5f,g). This suggests that HvMADS1 may repress the spike branching and that mutations in HvMADS1 caused the developmental delays in meristems assuming spikelet identity. The indeterminate branch meristems initiated from CSMs in *Hvmads1* spikes under high ambient temperatures continued to grow, forming branch-like structures (Fig. 2g and Extended Data Fig. 5d). Taken together, these results suggest that HvMADS1 maintains the

unbranched inflorescence shape at high temperatures by controlling meristem identity and development.

HvMADS1 represses ectopic cell division activity of meristems at high temperature. Meristem determinacy directs tissues to undergo programmed cell division and differentiation to maintain proper inflorescence architecture^{9–11}. To investigate how HvMADS1 affects cell division, we used 5-ethynyl-2'-deoxyuridine (EdU) to label S-phase nuclei during mitosis (Extended Data Fig. 6a). Young (W2.5) wild-type and *Hvmads1* (GP) spikes showed similar levels of cell division at control (15 °C) and high ambient temperatures (25 °C) (Extended Data Fig. 6b,c). As inflorescence development progressed, *Hvmads1* spikes at 25 °C exhibited additional mitotic activity at the rachilla position of CSMs or the boundary of CSMs (Fig. 3a), showing ectopic clusters of cell division in non-floret meristem regions of central spikelets (Extended Data Fig. 6c), consistent with the observed positions of ectopic organs. The EdU tracking assays thus revealed changes in the location of cell division in the meristems of the *Hvmads1* spikes under high temperature, probably associated with the phenotype of inflorescence-like meristems converting from rachillas, CSMs and/or ectopic meristems. Additionally, the cell division marker gene, *HvHistone4*, was expressed more broadly at the base of the CSM in *Hvmads1* at high temperatures, compared with tightly controlled expression at the CSM tips in wild-type tissues (Fig. 3b). High ambient temperatures thus induce ectopic cell division activity in *Hvmads1* CSMs. Moreover, HvMADS1 mRNA in wild-type spikes was expressed throughout the spike at W2.5, accumulating later in spikelet primordia and floral organs (Fig. 3c,d). Expression of the HvMADS1 protein in *pro::HvMADS1-eGFP* transgenic lines showed a similar pattern, found throughout the young inflorescence (W2.25–W3.5) (Fig. 3e) and accumulating later in central spikelets (W5) and floral organs, including the lemma, palea, anther and lodicule (Fig. 3f and Extended Data Fig. 7a). HvMADS1 thus seems to stabilize the meristem determinacy of cells from the central spikelet stimulated by high ambient temperatures, which represses cell division, thereby maintaining inflorescence shape; in *Hvmads1* spikes, meristem determinacy is reduced, and ectopic meristems develop into branches.

HvMADS1 coordinates thermal transcriptome programming of inflorescence meristems. To further probe how HvMADS1 regulates barley inflorescence thermomorphogenesis, we examined the impact of temperatures on HvMADS1 expression. Neither HvMADS1 mRNA nor protein levels were affected by temperature (Fig. 3g and Extended Data Fig. 7b–d), leading us to speculate that HvMADS1 maintains barley inflorescence morphogenesis in response to high ambient temperatures by modulating the expression of downstream genes. To test this possibility, we performed transcriptome analysis (RNA-seq) using inflorescence meristems at stages W2.5 (triple mound) and W3.5 (awn primordium) from wild-type (GP) and *Hvmads1* plants grown at 15 °C and 25 °C. Consistent with the obvious inflorescence defects of *Hvmads1* under high temperature, principal component analysis revealed that wild-type and mutant global transcriptional patterns diverged more at 25 °C at both developmental stages, and that principal component 1, which diverged more at high ambient temperature, explained 39.1% of the differences (Fig. 4a), highlighting an essential role of HvMADS1 in gene expression at the higher temperature. Correlation analysis confirmed significant dysregulation of thermal response genes and spike developmental genes at high ambient temperature in *Hvmads1* (Fig. 4b and Extended Data Fig. 8a). Gene transcription was generally inhibited in *Hvmads1* spikes (slope < 1), suggesting that HvMADS1 activates thermal response genes.

To investigate the molecular consequences of the loss of HvMADS1 function in barley inflorescence development and temperature response, we performed global transcriptional comparisons to

evaluate the possible correlation of gene expression with developmental phase, temperature, genotype and their interactions. In total, 9,434 differentially expressed genes (DEGs) were identified (Fig. 4c, Extended Data Fig. 8b and Supplementary Dataset 1). Of 3,194 DEGs affected by HvMADS1 expression (genotype), 2,568 (80.4%) were co-regulated by temperature (Fig. 4c). To investigate the interaction between HvMADS1 genotype and temperature, we compared the *Hvmads1* transcriptome at 25 °C with the *Hvmads1* transcriptome at 15 °C and the wild-type transcriptome at 25 °C by Venn diagram analysis. We found that 266 DEGs in W2.5 spikes and 476 DEGs in W3.5 spikes are likely to affect the mutant branching phenotype (Extended Data Fig. 8b). In agreement with phenotypic observations, the expression of transcripts affected by HvMADS1 at 25 °C was more distinct than at 15 °C. Co-expression cluster analysis based on developmental phase, temperature and genotype revealed 22 unsupervised groups of transcripts (Extended Data Fig. 8c and Supplementary Dataset 2). Clusters 6–13 contained meristem-associated and thermal response genes that were affected by all three variables. Genes in Clusters 1–5 and 15–19, encoding, for example, cell cycle/division and plant hormone pathway components, were co-regulated by temperature and HvMADS1. Clusters 14 and 22 included genes encoding receptor proteins and transcription factors that were affected only by HvMADS1 (Extended Data Fig. 8d and Supplementary Dataset 2). Gene ontology (GO) enrichment analysis indicated that DEGs at 15 °C were mainly involved in cellular component biosynthesis and nucleotide metabolism, whereas DEGs at 25 °C were largely associated with inflorescence development and regulation, meristem activity, cell cycle, stimulus response and gene expression (Fig. 4d and Supplementary Datasets 3 and 4), suggesting that HvMADS1 has different regulatory functions at 15 °C and 25 °C. We therefore conclude that HvMADS1 plays dominant roles in thermal transcriptome programming during barley inflorescence development. Due to the stable expression of HvMADS1 under control and high temperatures, the stability of spike architecture at high temperatures is probably achieved by changes in the targets of HvMADS1 but not in HvMADS1 itself. Other characteristics of HvMADS1, such as protein folding or binding affinity, may be affected by high temperature to regulate its downstream gene expression.

The most prominent changes in expression occurred in W3.5 *Hvmads1* spikes at 25 °C, for genes encoding meristem identity and transition regulators—that is, WUSCHEL-like, CLAVATA-like, TAWAWA-like, MADS-box, TEOSINTE BRANCHED (TCP transcription factors) and KNOX transcription factors (Extended Data Fig. 9a and Supplementary Dataset 5). These genes generally exhibited lower levels of transcription in *Hvmads1* spikes at 25 °C, confirmed by quantitative PCR with reverse transcription (RT-qPCR) (Extended Data Fig. 9b), which supports observations of delayed development of meristems in the mutant. TCP transcription factors play key roles in barley inflorescence development—that is, regulation by HvVRS5/int-C (INTERMEDIUM-C) of row type³⁶ and by HvCOM1/BDI1 (BRANCHED AND INDETERMINATE SPIKELET 1) in inflorescence architecture and meristem identity^{32,37}. The expression of several TCP family genes was downregulated in *Hvmads1* spikes at 25 °C (Extended Data Fig. 9a), implying that genes of this family may be involved in barley inflorescence thermomorphogenesis. However, the expression of other genes encoding key barley inflorescence regulators, such as HvCOM2 and the five HvVRS genes^{33,34,36,38–40}, was not significantly affected by HvMADS1 expression (Extended Data Fig. 9c), suggesting that HvMADS1-mediated inflorescence development is independent of known RAMOSA or conserved BD1 (Branched silkless 1, maize) or FZP (FRIZZY PANICLE, rice) pathways^{41–43}. Moreover, DEGs governing cell cycle progression, including *Cyclins*, *Histones*, *Cyclin-Dependent Protein Kinases* (CDKs) and *E2F* factors⁴⁴, figured prominently in the GO analysis at 25 °C but not at 15 °C (Fig. 4d), and they showed opposite

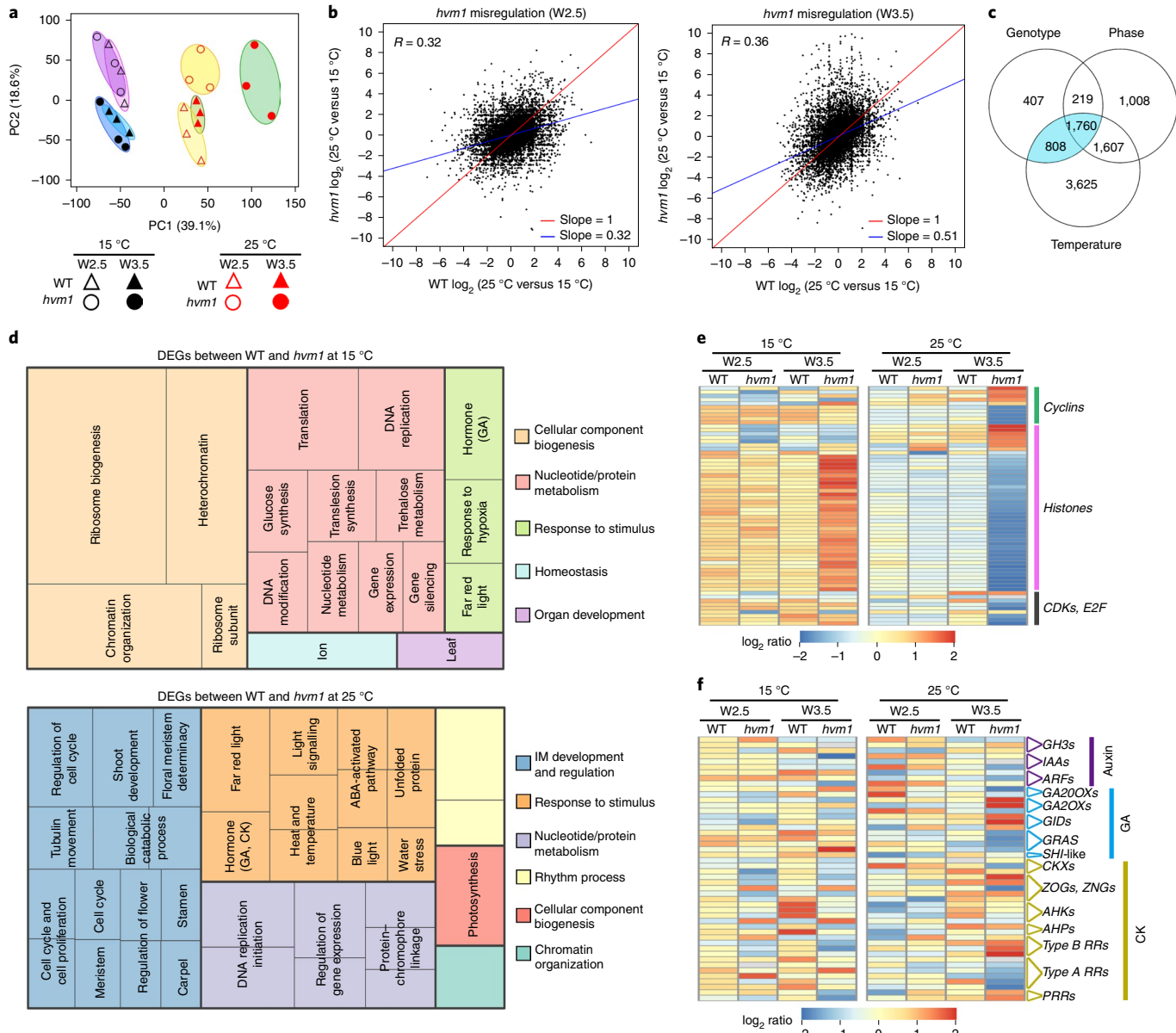


Fig. 4 | HvMADS1 coordinates thermal transcriptome programming of inflorescence meristems. **a**, Principal component (PC) analysis on the expression-filtered transcriptomes from W2.5 and W3.5 spikes of WT (GP) and *hvm1* plants grown at 15 °C and 25 °C. **b**, Correlation analyses showing the misregulation of thermal transcripts in *hvm1* compared with WT spikes at 25 °C at both W2.5 and W3.5 stages. **c**, Overlap of 9,434 DEGs due to temperature, genotype and developmental phase. The blue shading indicates genes co-regulated by genotype and temperature. **d**, GO analysis of DEGs between WT and *hvm1* spikes at 15 °C and 25 °C. GA, gibberellic acid. **e,f**, Hierarchical clustering analyses of DEGs that are relevant to cell cycle (**e**) and plant hormone signalling (**f**). GH3, *Gretchen Hagen 3*; IAA, Aux/IAA; ARF, Auxin Response Factor; GA20OXs, GA20 oxidases; GA2OXs, GA2 oxidases; GID, Gibberellin-Insensitive Dwarf; GRAS, GRAS-domain transcription factor; SHI, Short Internodes; ZOGs, CK O-glucosides; ZNG, CK N-glucosides; AHK, Histidine-kinase receptor; AHP, Histidine Phosphotransfer protein; PRR, Pseudo-response Regulator. Three biological repeats were performed per transcriptome.

expression patterns in *Hvmads1* spikes at the two temperatures (Fig. 4e and Supplementary Dataset 5), consistent with observed defects of meristem determinacy and cell cycle/division activity. DEGs associated with auxin, gibberellic acid and CK biosynthesis, metabolism and signalling also showed significant changes in *Hvmads1* at 25 °C compared with our other transcriptomes (Fig. 4f and Supplementary Dataset 5), consistent with the critical role of these three hormones in barley inflorescence development³⁹.

The barley homologues of *Arabidopsis* *PHYB* and *PIF4* with reported functions in perceiving temperature and thermomorphogenesis^{4,5,7,8} showed reduced expression levels in *Hvmads1* spikes, particularly at 25 °C (Extended Data Fig. 9a,d and Supplementary

Dataset 5). Moreover, changes in *Histone* gene expression in *Hvmads1* spikes between 15 °C and 25 °C imply that HvMADS1 probably involves chromatin remodelling to control thermal transcription (Fig. 4e). In *Arabidopsis*, Histone variant H2A.Z has been reported to regulate nucleosome occupancy of thermal transcription^{4–6}. It is noteworthy that a large number of *Heat Shock Protein* genes⁴ and heat tolerance players (that is, *ERECTA* and *Thermo-Tolerance 1*)^{45,46} showed large variability of transcription in *Hvmads1* spikes at 25 °C compared with the wild type (Extended Data Fig. 9a,d and Supplementary Dataset 5), consistent with the dysregulation of global thermal responsive gene expression in *Hvmads1* (Fig. 4b and Extended Data Fig. 8a).

HvMADS1 binds to the CArG-box to regulate gene transcription in response to temperature. SEP proteins regulate the transcription of target genes by binding to A-tract-rich CArG-box motifs^{24,25}, which change conformation with temperature *in vitro*^{26–28}. In *A. thaliana*, the *in vitro* binding affinity of SEP3 to A-tract CArG-boxes increases with temperature, but binding to non-A-tract CArG-boxes remains temperature-independent²⁵. To test whether A-tract sequences affect temperature-dependent transcriptional activation by HvMADS1, we made artificial promoters carrying A-tract or non-A-tract CArG-boxes for *in vivo* dual-luciferase assays and *in vitro* electrophoretic mobility shift assays (EMSA) under different temperature conditions (Fig. 5a). HvMADS3, the homologue of *Arabidopsis* AGAMOUS (known to regulate gene expression via CArG-boxes independent of temperature), was used as a control²⁵. HvMADS1 exhibited temperature-dependent gene activation via A-tract CArG-boxes only; the activation of A-tract CArG-boxes by HvMADS3 at both low and high temperatures demonstrated that temperature-dependent transcription activity of HvMADS1 is not shared with other non-SEP MADS-box proteins, such as HvMADS3 (Fig. 5b,c). EMSAs demonstrated increased binding of A-tract CArG-boxes by homodimeric and monomeric HvMADS1 at elevated temperatures (Fig. 5d), and *in vivo* co-immunoprecipitation assays showed that HvMADS1 can form homodimers in tobacco cells (Fig. 5e). Chromatin immunoprecipitation (ChIP)-PCR analysis of four putative thermal and developmental regulators, HvPIF4 (ref. ⁸), HvRPK4 (*RECEPTOR-LIKE PROTEIN KINASE 4*), HvTFL1L (*TERMINAL FLOWER 1-like*) and HvTB1L (*TEOSINTE BRANCHED 1-like*), with promoters containing A-tract CArG-boxes revealed that HvMADS1 binding increased with temperature (Fig. 5f), consistent with decreased expression of these genes in *Hvmads1* spikes at high ambient temperature (Extended Data Fig. 9a,b,d). We have thus demonstrated an *in planta* mechanism by which a MADS-box protein regulates gene expression via temperature-dependent binding to A-tract CArG-boxes to promote the transcription of downstream response genes.

HvMADS1 integrates CK homeostasis and temperature response to regulate barley inflorescence branching. Plant hormones, including auxin, gibberellic acid and CK, are implicated in the control of plant architecture and inflorescence meristem activity^{9,10,39}. Notably, of the hormone-related DEGs in our transcriptomic data (Fig. 4f and Supplementary Dataset 5), two-component signalling *response regulators* (RRs) of CK⁴⁷, type A and type B, had opposite responses to high ambient temperature in *Hvmads1* spikes (Fig. 6a). Genes encoding type A RRs (repressed by the CK response) were downregulated in *Hvmads1* spikes at 25 °C, whereas genes encoding type B RRs (activated by the CK response) were upregulated, suggesting an enhanced CK response in *Hvmads1* plants at high temperature.

To examine how CK affects barley inflorescence development, wild-type and mutant spikes from W1–W5 were treated with the CK analogue benzylaminopurine (BAP). At 15 °C, *Hvmads1* spikes produced several EI meristems (about ten in *Hvmads1*) (Fig. 6b,c), which phenocopied *Hvmads1* inflorescences at high temperatures in the absence of BAP (Fig. 2b). At 28 °C, BAP also induced ES meristems from the lemma side of the central spikelet in both wild-type and *Hvmads1* spikes, and EIs in the central spikelet from the palea side of *Hvmads1* spikes only (Fig. 6d,e). We therefore propose that altered CK homeostasis may contribute to the abnormal ectopic branching phenotype of *Hvmads1* spikes at high temperature.

The measurement of endogenous CK levels by liquid chromatography–tandem mass spectrometry revealed that active CK forms (that is, isopentenyladenine and *trans*-zeatin) and CK metabolites were significantly increased in *Hvmads1* spikes, with higher levels at 28 °C than at 15 °C (Fig. 6f). To monitor *in vivo* CK levels,

we introduced a synthetic CK biosensor construct (*pTCS::YFPn*) into wild-type (WI) and *Hvmads1*/WI plants. At 15 °C, the CK-responsive YFP signal accumulated in spikelet meristems, while at 28 °C, a higher CK response was observed in the inflorescence main axis, which was both wider and earlier in *Hvmads1* spikes (Fig. 6g). Importantly, an ectopic CK response was observed at the base of the central spikelet and at the main axis at 28 °C (Fig. 6g), which may contribute to indeterminacy in the adjacent meristems, mimicking ectopic branch meristem formation and cell cycle/division activity in *Hvmads1* spikes (Fig. 3a,b). These findings suggest that HvMADS1 promotes the decay of CK molecules to maintain hormone homeostasis that inhibits ectopic meristem activity in barley inflorescence at high ambient temperatures.

HvMADS1 directs HvCKX3 to regulate spike determinacy under high temperatures. CYTOKININ OXIDASE/DEHYDROGENASE (CKX) proteins degrade CK to maintain hormonal homeostasis in response to environmental and developmental cues⁴⁶. The changed flow of CK metabolites (for example, isopentenyladenine N-glucoside and *trans*-zeatin O-glucoside) (Fig. 6f) and enhanced CK response in *Hvmads1* plants are consistent with findings of altered CK homeostasis from rice and *Arabidopsis* plants with altered CKX expression^{48,49}. Three HvCKX genes were also identified as DEGs in *Hvmads1* spikes (Supplementary Dataset 5). One of them, HvCKX3 (HORVU1Hr1G042360), is predominantly expressed in early spike (W2–3.5) development³⁰.

ChIP-PCR analysis targeting the CArG-boxes in the promoter and intron regions of HvCKX3 using *pro:HvMADS1-eGFP* transgenic plants confirmed that HvMADS1 bound all HvCKX3 promoter fragments containing CArG-box sequences *in vivo*, but only binding of A-tract CArG-boxes improved with high temperatures (Fig. 7a). EMSAs confirmed the result *in vitro* (Fig. 7b), and *in vivo* dual-luciferase assays showed that improved binding of HvCKX3 promoter by HvMADS1 at high ambient temperature and heat stress conditions led to increased reporter gene transcription (Fig. 7c and Extended Data Fig. 10), consistent with artificial A-tract CArG-box assays (Fig. 5a–d). Accordingly, the expression level of HvCKX3 was lower in *Hvmads1* spikes and increased with temperature in wild-type but not in *Hvmads1* spikes (Fig. 7d). *In situ* hybridization assays also demonstrated that temperature-induced accumulation of HvCKX3 mRNA occurred at the tip and base of CSMs and the joints between the CSM and main axis in wild-type spikes (Fig. 7e). Furthermore, an *Hvckx3* mutant created by CRISPR-Cas9 consistently showed EI formation and reduced meristem determinacy at high ambient temperature (25 °C) and heat stress (28 °C) conditions (Fig. 7f,g), mimicking the defects of *Hvmads1*. Similar to the *Hvmads1* mutant, the *Hvckx3* spike did not show ectopic branches or spikelets at 15 °C (Fig. 7g), suggesting that HvMADS1 affects local excessive CK flow and metabolism during spike development by activating the expression of HvCKX3 only under high-temperature conditions (Fig. 7d,e). These results demonstrate that HvMADS1 controls CK homeostasis at high temperature to stabilize barley spike morphogenesis via HvCKX3.

Conserved HvMADS1 sequence in barley varieties. To assess the natural variation of HvMADS1, we investigated the sequences of HvMADS1 encoding and regulatory regions in selected barley cultivars. Analysis of exome sequencing data across 267 barley genotypes identified only three synonymous and one non-synonymous single nucleotide polymorphisms (SNPs) in the C-terminal domain, and no SNPs in any other domains, of HvMADS1 (Supplementary Fig. 1 and Supplementary Dataset 6)⁵⁰. Further sequencing of 101 wild and cultivated barley varieties from different countries showed no further SNPs in the HvMADS1 coding region and first intron (Supplementary Dataset 7), revealing strong conservation of the HvMADS1 sequence during domestication.

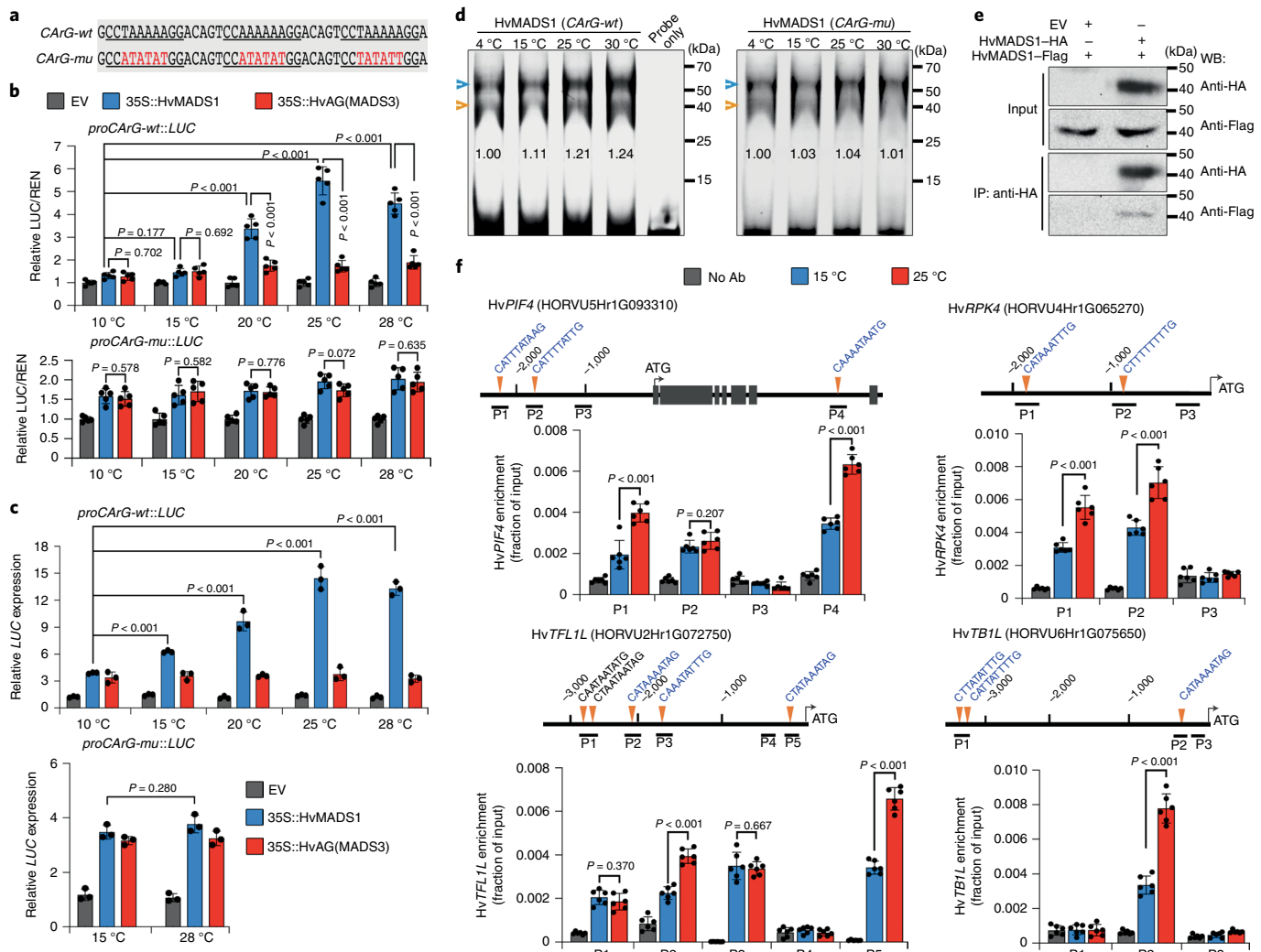


Fig. 5 | HvMADS1 binds to the CArG-box to regulate gene transcription in response to temperature. **a**, Artificial CArG-boxes with A-tracts (underlined, CArG-wt, wild-type) or non-A-tracts (red, CArG-mu, mutant) used to drive luciferase (LUC) gene expression. **b**, Normalized luciferase activity (LUC/REN) activated by artificial CArG-box promoters (from **a**) in the presence of HvMADS1, HvMADS3 (temperature-independent gene activation) or empty vector (EV, negative control). REN, Renilla luciferase (internal control). The data are shown as mean \pm s.d.; $n=5$ biological replicates. **c**, RT-qPCR analysis of reporter gene LUC expression from **a** and **b**. The values are normalized to REN expression. The data are shown as mean \pm s.d.; $n=3$ biological replicates. **d**, EMSA of HvMADS1 with DNA fragments containing CArG-wt and CArG-mu boxes (from **a**) at different temperatures. Homodimeric (blue arrowheads) and monomeric (orange arrowheads) HvMADS1 protein-DNA complexes are indicated. Quantification of band intensity is shown on each gel. **e**, In vivo co-immunoprecipitation assay showing the homodimers of HvMADS1. Tobacco leaf extracts that transiently expressed HvMADS1-Flag (tag) with HvMADS1-HA or with EV (negative control) were immunoprecipitated by anti-HA antibody. WB, western blot; IP, immunoprecipitation. **f**, ChIP-PCR assays of the regulatory regions of four selected genes from *pro:HvMADS1-eGFP* transgenic plants grown at 15 °C and 25 °C. The promoter or intron regions containing A-tract (blue text) and non-A-tract (black text) CArG-boxes of HvPf4 (*Phytochrome-Interacting Factor*), HvRPK4, HvTFL1L and HvTB1L are indicated. The data are shown as mean \pm s.d.; $n=6$ independent experiments. No antibody (No Ab) served as a negative control. The *P* values indicate the results from pairwise comparisons of one-way ANOVA tests (**b,c,f**). All experiments were repeated independently at least three times, with similar results.

Discussion

Global warming has been affecting numerous plant species, including their distribution, phenology and biodiversity^{1,2,14}. The developmental plasticity of the inflorescence is also probably regulated by temperature conditions^{2,3,12,13}. Here, we have shown that a barley SEP protein, HvMADS1, maintains branchless inflorescence development under high ambient temperatures via the control of CK homeostasis (Fig. 7h). The development of ectopic meristems in the *Hvmads1* mutant is regulated by a genotype \times environment interaction, a phenomenon not previously observed in reports of plant thermomorphogenesis. Furthermore, our data reveal that HvMADS1 fulfills its pivotal function in thermal response by controlling

transcriptional changes that regulate meristem identity and development, probably through improved binding to promoters via A-tract CArG-boxes, whose physical conformations change with temperature^{25–28}. These findings reveal a role for MADS-box proteins in directing inflorescence architecture through temperature-sensitive regulation of a myriad of regulatory and cellular functions, which extends the recognized function of plant MADS-box genes as determinants of floret identity^{19,20}.

E-class SEP genes are broadly involved in specifying all whorls of floral organs and in floral determinacy^{9–11,20}. Our genetic and phenotypic analyses revealed that the loss of HvMADS1 affected only awn elongation at control temperatures, suggesting functional

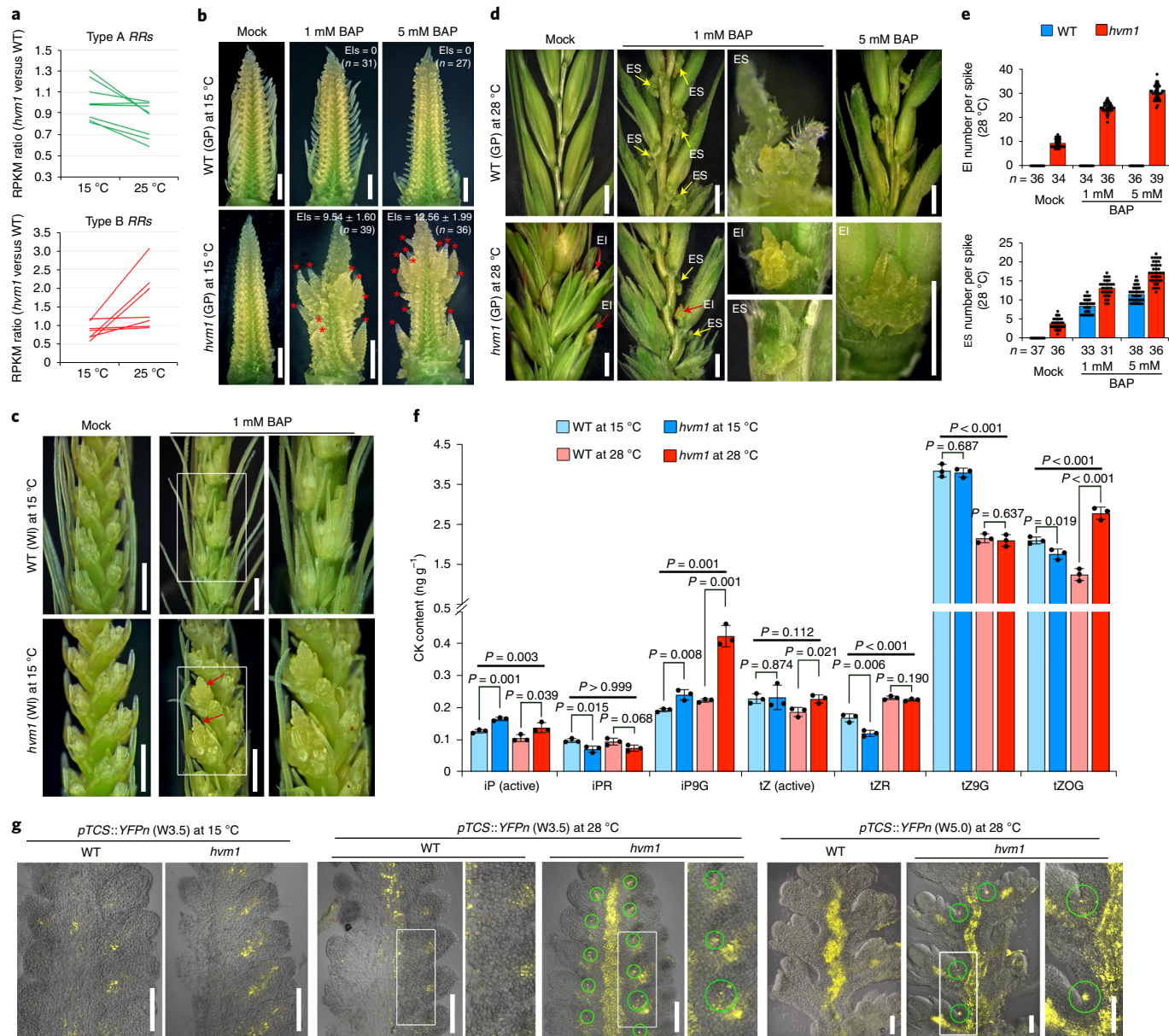


Fig. 6 | HvMADS1 integrates CK signalling and temperature response to regulate barley inflorescence branching. **a**, Read counts per kilobase per million (RPKM) ratio for CK two-component signalling genes (eight type A RRs and seven type B RRs) in W3.5 spikes. A ratio greater than 1 indicates upregulated expression in the *hvm1* mutant; $n=3$ biological replicates. **b**, WT (GP) and *hvm1* spikes after BAP treatments at 15 °C. The red asterisks indicate Els. Scale bars, 1 mm. **c**, Phenotypes of WT (WI) and *hvm1* spikes after BAP treatment at 15 °C. The arrows indicate Els. Scale bars, 1 mm. **d**, Phenotypes of WT (GP) and *hvm1* spikes after BAP treatment at 28 °C. ESs (yellow arrows) attached to the lemma are observed in WT and *hvm1* spikes, but Els (red arrows) attached to the palea are detected only in *hvm1* spikes. WT lateral spikelets under mock treatment have been removed. Scale bars, 2 mm. **e**, Average number of Els (top) and ESs (bottom) per spike after BAP treatment. The data are shown as mean \pm s.d. **f**, Quantification of endogenous CK content in W3.5 spikes. iP, isopentenyladenine; iPR, isopentenyladenine riboside; iP9G, isopentenyladenine 9-N-glucoside; tZ, *trans*-zeatin; tZR, *trans*-zeatin riboside; tZ9G, *trans*-zeatin 9-N-glucoside; tZOG, *trans*-zeatin O-glucoside. The data are shown as mean \pm s.d.; $n=3$ biological replicates. The *P* values indicate the results from pairwise comparisons of one-way and two-way ANOVA tests. **g**, WT (WI) and *hvm1* spikes expressing *pTCS::YFPn* (CK biosensor, yellow signals). Heat treatment at 28 °C was for seven days. The green circles indicate ectopic signals. Scale bars, 100 μ m. All experiments were repeated independently at least three times, with similar results.

redundancy of HvMADS1 with other SEP/MADS proteins. However, in other grasses, such as rice, the *Osmads1* mutant exhibits elongated leafy paleas and lemmas and defective inner organs^{29,51,52}, which is different from the barley *Hvmads1* mutant, indicating functional diversity of HvMADS1 compared with *MADS1* orthologues in other grasses. SEP proteins play a redundant role in regulating plant inflorescence architecture by forming multimeric protein

complexes as reported in *Arabidopsis*, rice and tomato^{21,23}. Notably, barley *lofsep* double mutants (*Hvmads1/5* and *Hvmads1/34*) did not show obvious inflorescence phenotypic differences compared with *Hvmads1* single mutants in response to high temperatures. Future work on the generation and analysis of the triple mutant of HvMADS1, HvMADS5 and HvMADS34 may elucidate *LOFSEP* functional redundancy. Besides the *LOFSEPs*, two barley *SEP3*-like

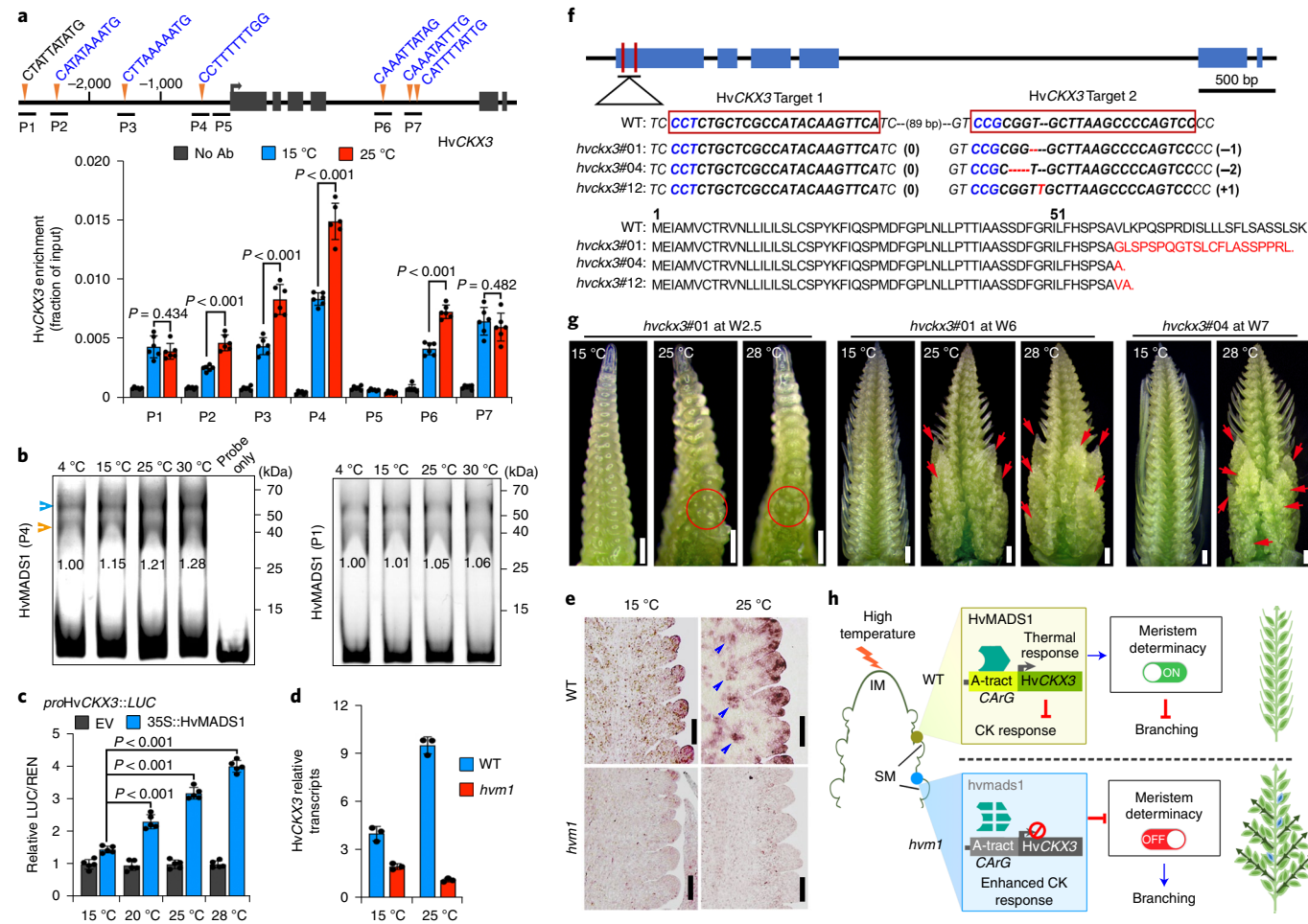


Fig. 7 | HvMADS1 directs HvCKX3 to regulate spike determinacy under high temperatures. **a**, In vivo binding of HvCKX3 CArG-boxes by HvMADS1 at 15 °C and 25 °C. Top, HvCKX3 genomic region containing A-tract (blue text) and non-A-tract (black text) CArG-boxes. Bottom, seven DNA fragments tested by ChIP-PCR. The data are shown as mean \pm s.d.; n = 6 independent experiments. No Ab is the negative control. The P values indicate the results from pairwise comparisons of one-way ANOVA tests. **b**, EMSA assays of HvMADS1 with HvCKX3 promoter fragments containing A-tract (P4) and non-A-tract (P1) CArG-boxes at various temperatures. Homodimeric (blue arrowhead) and monomeric (orange arrowhead) protein-DNA complexes are indicated. Quantification of band intensity is shown on each gel. **c**, Normalized luciferase activity (LUC/REN) activated by the HvCKX3 promoter in tobacco cells in the presence of HvMADS1 or EV (negative control). The data are shown as mean \pm s.d.; n = 5 biological replicates. The P values indicate the results from pairwise comparisons of one-way ANOVA tests. **d**, HvCKX3 transcript levels in WT (GP) and *hvm1* spikes at 15 °C and 25 °C. The data are shown as mean \pm s.d.; n = 3 biological replicates. **e**, In situ hybridization of HvCKX3 in wild-type and *Hvmads1* spikes at 15 °C and 25 °C. Scale bars, 100 µm. The blue arrowheads indicate mRNA accumulation at the base of the CSM. **f**, Creation of the *Hvckx3* mutant using CRISPR-Cas9. Top, two targets (T1 and T2) in the first exon of HvCKX3. Bottom, DNA sequences and putative encoded amino acid sequences of three independent T_0 transgenics in the WT (GP). **g**, Phenotypes of *Hvckx3* spikes at stages W2.5, W6 and W7 in response to high temperatures. The red circles indicate abnormal differentiation of spikelet meristems. The red arrows indicate EIs. Scale bars, 200 µm. **h**, Proposed model of HvMADS1-mediated spike determinacy maintenance at high temperatures. HvCKX3 expression is activated by HvMADS1 to drive CK homeostasis, which stabilizes meristem determinacy. In *hvm1* spikes, the lack of HvCKX3 activation causes enhanced CK response and reduced meristem determinacy, triggering ectopic branching. SM, spikelet meristem. All experiments were repeated independently at least three times, with similar results.

genes, HvMADS7 and HvMADS8, are highly expressed in developing inflorescences³⁰, and their orthologues in *Arabidopsis* and rice are required for proper floret organ identity^{19,20,53}. Further investigation of barley *SEP3*-like genes in inflorescence development under different temperature conditions will provide a mechanistic picture of *SEP* gene function in inflorescence thermomorphogenesis.

Our work reveals that HvMADS1 regulates the thermal transcriptome to repress cell cycle/division activity and maintain CK homeostasis at high ambient temperatures. The application of a CK analogue induced ectopic organ formation in *Hvmads1* spikes at control temperatures (Fig. 6b,c), leading to the identification of HvCKX3 as an HvMADS1 target. In the absence of HvMADS1, insufficient levels of HvCKX3 cannot maintain local CK homeostasis

at high temperatures, leading to reduced meristem determinacy and changed meristem identity, ectopic cell division for branch meristems, and ultimately, the development of a branched inflorescence (Fig. 7h). At high temperatures, an *Hvckx3* mutant phenocopied *Hvmads1* (Fig. 7g), further supporting our conclusion that HvMADS1 integrates thermal response and CK homeostasis to maintain inflorescence architecture via HvCKX3. At control temperatures, HvMADS1 also regulates HvCKX3 expression; the challenging of barley spikes with ectopic CK produced a branched-inflorescence-like phenotype only in the *Hvmads1* mutant. In *Arabidopsis*, high temperatures affect developmental plasticity, including the promotion of hypocotyl elongation and flowering time regulated mainly by the PHYB-PIF4 pathway^{4,5,7,8}.

In barley, however, thermally induced inflorescence branching does not occur in wild-type plants due to the regulatory effect of HvMADS1. The loss of HvMADS1 led to a change in the morphogenesis of the spike, altered the expression of barley homologues of *PHYB* and *PIF4*, and induced a large number of *Heat Shock Protein* and *Histone* genes under high temperatures. The details of the HvMADS1 association with the PHYB–PIF4 regulatory network, heat stress response and chromatin remodelling-mediated thermal transcription in barley must await future investigation.

Seasonal temperature changes affect plant growth, flowering time and phenotypic plasticity^{2,3,12,15}. A severe consequence of climate change is the projected increase in temperature, posing a significant challenge for maintaining agricultural crop yield and quality^{17,18}. A better understanding of the mechanisms underpinning desirable plant traits in response to temperature can therefore offer insights into breeding climate-smart plants to sustain productivity^{1,12,15}. The branches of *Hvmads1*, which developed from ectopic meristems initiated after the formation of spikelet meristems, are not comparable to panicle-like inflorescences in grasses such as rice, because the branch meristems in rice are initiated before the spikelet meristems^{9–11}, suggesting possible diverse mechanisms regulating branching versus non-branching inflorescence in grasses. The variability of MADS1 in directing temperature response in different grass crops remains to be investigated. Temperature-dependent binding of SEPs (and possibly other MADS-box proteins) to promoters is likely to regulate plant thermomorphogenesis, representing a biological control tool as yet unexploited in crop plants. Our findings provide mechanistic insights into the development of diverse grass inflorescence architectures in response to climate, which reveal new avenues for breeding climate-smart plants to overcome the traditional compromise between heat tolerance and high yield.

Methods

Plant materials and generation of transgenic plants. The wild-type barley (*Hordeum vulgare*) varieties used included GP (United Kingdom), WI (South Australia) and Vla (Western Australia). A monocot-specific robust CRISPR–Cas9 system was used to create the barley mutants³¹. Two target sequences for each HvMADS gene were selected within the MADS domain. A Blast search (https://webblast.ipk-gatersleben.de/barley_ibsc/) of the target sequences (including the protospacer adjacent motif NGG) was performed to confirm their targeting specificity in the barley genome⁵⁴. The target sites of three *SEPALLATA* genes (HvMADS1, HvMADS5 and HvMADS34) and HvCKX3 were sequenced in GP, and HvMADS1 target sites were also sequenced in WI and Vla, all showing 100% identity with the reference (*Morex*) genome⁵⁴. Single guide RNA (sgRNA) T1 was driven by rice promoter OsU6a, and sgRNA-T2 was driven by rice promoter OsU6b. The sgRNA expression cassettes of OsU6a–sgRNA-T1 and OsU6b–sgRNA-T2 were amplified from pYLsgRNA-OsU6a and pYLsgRNA-OsU6b templates using Phusion High-Fidelity DNA Polymerase (New England BioLabs) and cloned into a binary vector, pYLCRISPR–Cas9^{Fluo}-H, using *Bsa*I as described in ref.³¹. sgRNA-T1 of HvMADS1 and sgRNA-T2 of HvMADS5 were used for HvMADS1/5 construction to create the double mutant, sgRNA-T1 of HvMADS1 and sgRNA-T2 of HvMADS34 were used for HvMADS1/34 constructs, and sgRNA-T1 of HvMADS5 and sgRNA-T2 of HvMADS34 were used for HvMADS5/34 constructs (Extended Data Fig. 1). All constructs were used for *Agrobacterium tumefaciens* AGL1-mediated transformation of immature barley embryos as previously described³⁵: HvMADS1 into GP, Vla and WI varieties, and HvMADS5, HvMADS34, HvMADS1/5, HvMADS1/34, HvMADS5/34 and HvCKX3 into GP only. Independent *T*₀ plants carrying biallelic and homozygous mutations were identified by genotyping using a Phire Plant Direct PCR Kit (Thermo Fisher Scientific) and Sanger sequencing (AGRIF). The editing efficiency of biallelic mutation, heterozygous and homozygous for three *SEPALLATA* genes in single and double mutants, is listed in Supplementary Table 1. All primers used for CRISPR–Cas9 constructs are listed in Supplementary Table 2.

To analyse HvMADS1 protein accumulation and regulation, the *pro::HvMADS1-eGFP* construct was created by inserting the 2,489-base-pair (bp) HvMADS1 promoter and full-length HvMADS1 cDNA fused with *eGFP* (enhanced green fluorescent protein) into the *Kpn*I and *Bst*EII sites of pCAMBIA1301, using In-Fusion (Takara) cloning technology. The vector was transformed into barley variety GP using *A. tumefaciens* AGL1-mediated transformation as described above. At least three independent lines were used for analysis. The primers are listed in Supplementary Table 3.

A CK biosensor (*pTCS::YFPn*) was designed using a 3×YFP (Yellow Fluorescent Protein) reporter with a nuclear localization sequence (*n*) driven by an artificial CK-responsive two-component system promoter (*pTCS*) combined with a 35S minimal promoter. The *pTCSn-35Smin* sequence was synthesized in pUC57 by Genscript on the basis of the *pTCSn1::GFP-ER* vector⁵⁶. The synthesized fragment was flanked by 5'-*Hind*III and 3'-*Kpn*I restriction sites, allowing it to be cloned into the Gateway-compatible pMDC32 vector in place of the double 35S promoter. A 2.6-kilobase 3×YFPn gene, optimized for use in barley, was transferred into the *pTCSn1::pMDC32* vector using LR clonase II (Thermo Fisher Scientific) as described in refs.^{57,58}. The resulting *pTCS::YFPn* vector was transformed into barley variety WI using *A. tumefaciens* AGL1 as described above. Eighteen *T*₀ plants were identified with ideal YFP signals. Three independent lines were crossed with the *Hvmads1*/WI lines. *T*₁ offspring carrying both the *Hvmads1* mutation and YFP CK sensor were used for further CK response analysis.

Plant growth and temperature treatments. Barley grains were set in cocopeat soil, germinated and grown in 15 °C light, 10 °C dark conditions (control temperatures) with a 16 h photoperiod at 50% humidity in growth chambers (Plant Accelerator, Waite Campus, University of Adelaide, Australia). In all experiments, the night (dark) temperature was 5 °C below the day (light) temperature. For temperature treatments of wild-type, *Hvmads1*, *Hvckx3*, *pro::HvMADS1-eGFP* and *pTCS::YFPn* plants, the plants were germinated and grown at control temperatures (15 °C light/10 °C dark) conditions to W1 (Waddington stage)³⁵ and then moved to different day temperatures (20 °C, 23 °C, 25 °C or 28 °C) for phenotype or fluorescent signal investigation. For the examination of dosage effects of temperature on inflorescence development (Fig. 2a–c), the plants were moved back to 15 °C day temperature at W7 for spike observation, but for all other experiments, the plants were grown to maturity at the experimental temperature conditions.

Nicotiana benthamiana plants were grown in a greenhouse at 23 °C with a 16 h period. The plants were grown until they had six leaves, when the youngest leaves >1 cm long were infiltrated with *A. tumefaciens*. The transformed plants were maintained in growth chambers at 10 °C, 15 °C, 20 °C, 25 °C or 28 °C for the duration of the experiment.

Plant phenotyping and scanning electron microscopy. Inflorescence development in wild-type and *Hvmads1* spikes was photographed using a stereomicroscope with a digital camera (Leica, MZ FLIII). The barley spikes were photographed using a Nikon D5600 digital camera. Different Waddington stages of immature spike tissues from various temperatures were used for scanning electron microscopy (Philips, XL30 FEG) as previously described⁴³, and photographs were taken with an optical microscope (Ni-E, Nikon).

Microscopy and image processing. All confocal fluorescent images were recorded with a digital camera mounted to an A1R Laser Scanning Confocal Microscope (Nikon) using a fluorescein-isothiocyanate-specific filter (EdU and eGFP; excitation, 488 nm; emission, 505–520 nm), a PI filter (excitation, 561 nm; emission, 590–640 nm), a YFP filter (excitation, 514 nm; emission, 520–535 nm) or a differential interference contrast filter. The dissection of *pTCS::YFPn* inflorescences was performed as previously described³⁹. The images were extracted with NIS-Elements Viewer versions 4.20 and 4.30.01 (Nikon).

EdU labelling. EdU staining was performed as described in refs.^{60,61}, with the following modifications (Extended Data Fig. 6a). Briefly, leaves and sheaths were removed carefully before treatment. Intact inflorescences were incubated with 10 μM EdU for 30 min in the growth chamber and fixed with 0.5 ml of fixative (100% ethanol, 0.1% (v/v) Triton X-100) for 30 min at room temperature. The samples were washed with 1× PBS (3 × 10 min), incubated in EdU detection cocktail (Alexa Fluor Azide reaction, Life Technologies) for 30 min in the dark and washed again with 1× PBS (3 × 10 min). The samples were incubated with PI solution (20 μg ml⁻¹ PI in PBS) for 30 min at room temperature and washed in 1× PBS (3 × 10 min) before observation by confocal microscope.

RNA extraction and RT-qPCR. Total RNA was isolated from barley tissues and *N. benthamiana* leaf samples using TRIzol reagent (Life Technologies). 2 μg of total RNA was incubated with 1 U of DNaseI (Fermentas) in a total volume of 10 μl at 37 °C for 15 min. cDNA was generated using 200 U of Moloney murine leukaemia virus reverse transcriptase (ThermoFisher) and 2.5 μM oligo-dT primer, according to the manufacturer's instructions. Diluted cDNA was used as a template for real-time RT-qPCR with a 384-well QuantStudio Flex 6 (Thermo Fisher Scientific) machine as previously described⁴². The RT-qPCR data for each target gene are presented as average expression levels from at least three biological replicates, each with three technical replicates. Gene expression is normalized to the expression levels of housekeeping genes: HvActin7 and HvEF2 for barley or the REN gene for *N. benthamiana* leaf samples. All primers used for RT-qPCR are listed in Supplementary Table 4.

Immunoblotting of HvMADS1. Total protein from W3.5 spikes collected from three independent *pro::HvMADS1-eGFP* lines were extracted using 1× Passive Lysis buffer (Promega). The protein samples were separated by SDS-PAGE on 12%

acrylamide midi-gels (Bio-Rad) and transferred onto a polyvinylidene difluoride membrane (Bio-Rad). The membrane was incubated with monoclonal anti-GFP (1:1,000 dilution; ABclonal; catalogue number, AE012) or anti-tubulin (1:2,000 dilution; Merck; catalogue number, 05-661) primary antibodies and secondary antibody conjugated to horseradish peroxidase (1:5,000 dilution; Cell Signaling Technology; catalogue number, 0706) as previously described⁶². Detection was performed with the Chemidoc MP Imaging System (Bio-Rad) using SuperSignal West Pico chemiluminescent substrate (Pierce).

In situ mRNA hybridization analysis. Spikes collected at early stages were prepared for *in situ* hybridization as previously described⁶³. Probe templates of 315 bp from HvMADS1 cDNA (205–540 bp), 302 bp from HvCKX3 cDNA (1,113–1,415 bp) and full-length coding sequence of HvHistone4 were amplified by PCR using specific primers fused with the T7 promoter (the primers are listed in Supplementary Table 5). Digoxigenin-labelled antisense and sense probes were synthesized using primers incorporating the T7 polymerase binding site at the 5' end using an *in vitro* transcription kit (Roche) according to the manufacturer's instructions. Hybridization with 2.5 ng μl^{-1} digoxigenin-labelled RNA probes, post-hybridization washes and immunodetection were performed automatically using an InSituPro VSi robot (Intavis). The slides were incubated with diluted (1:1,000) antibody conjugate (anti-digoxigenin-AP; Roche; catalogue number, 11093274910) in BSA wash solution, then washed in BSA wash solution (3 \times 15 min). Images were obtained using an optical microscope (Ni-E, Nikon). The empty slide background was colour-matched in Photoshop (Adobe) to compare between separate slides.

RNA-seq library preparation. Inflorescence samples of wild-type (GP) and Hvmads1 plants grown at 15 °C/10 °C (day/night) and 25 °C/20 °C were collected at W2.5 and W3.5. Total RNA was extracted from 15–20 spikes for each of three biological replicates using TRIzol (Invitrogen) and purified using an RNeasy Micro Kit (Qiagen) following the manufacturer's instructions. RNA quality and integrity were assessed on the Agilent 2200 TapeStation. Library preparation was performed using 1 μg of high-integrity total RNA (RNA integrity number > 8) using the TruSeq RNA Library Preparation Kit v.2 (Illumina, RS-122-2101 and RS-122-2001), following the manufacturer's instructions. The libraries were sequenced using paired-end sequencing of 250–300 bp fragments on a HiSeq4000 at Novogene.

Analysis of RNA-seq data. The quality of raw sequencing reads for all samples was examined using FastQC (version 0.11.4; <http://www.bioinformatics.babraham.ac.uk/projects/fastqc/>)⁶⁴. Reads with adaptors and of low quality (>20% bases with quality score <15) were removed using Trimmomatic software (version 0.38)⁶⁵, and reads composed of >5% unknown bases (labelled N) were discarded. Fragments per kilobase per million were normalized by genome-wide coverage. Clean reads were mapped to the barley reference genome (2017 Morex genome, http://webblast.ipk-gatersleben.de/barley_ibsc/) using HISAT2 aligner (version 2.0.0)^{54,66}. RPKM was normalized using HTSeq (version 0.11.2)⁶⁷.

Analysis was conducted on 39,734 high-confidence genes detected. Principal component analysis was performed using the regularized-logarithm transformation for read count data using custom R scripts. Scatter plots were generated using \log_2 fold change (from 25 °C to 15 °C), and linear relationships were calculated using a custom R script^{7,68}.

DEGs were identified using the R package DESeq2 (version 3.11)⁶⁹, following the model \sim genotype \times temperature \times phase to account for the genotype (wild-type or Hvmads1), the temperature at harvesting (15 °C or 25 °C) and the developmental stage (W2.5 or W3.5), as well as their interactions. The model enabled the identification of the contributions of (1) the genotype variable, (2) the temperature variable, (3) the phase variable and (4) their interaction terms; that is, whenever a change in one of the variables has a direct effect on the other. The raw data counts were normalized and transformed to estimate the mean and variance^{7,67}. Results for the pairwise comparisons of any two variables were extracted to investigate the effects of genes. The Benjamini–Hochberg adjustment was implemented to compute adjusted *P* values, and false-discovery-rate-adjusted *P* values were used to assess significance; a common threshold of 1% was used throughout. In total, 9,434 DEGs were identified (Supplementary Dataset 1) and annotated on the basis of BLASTx alignments against protein databases of *Arabidopsis* (TAIR10_peptide; <http://www.arabidopsis.org/>) and rice (MSU7_peptide; <http://rice.plantbiology.msu.edu/>). Clustering was performed as previously described (<http://research.microsoft.com/apps/pubs/default.aspx?id=67239>)⁷, to model clusters without prior restrictions. Using the coseq Bioconductor package (version 1.0.1)⁷⁰, a Gaussian mixture model was fit to the arcsine-transformed normalized profiles of differentially expressed contigs for $k = 2, \dots, 100$ clusters. On the basis of the integrated completed likelihood criterion for model selection⁷, the model with $k = 22$ clusters was selected for unsupervised assembly (Supplementary Dataset 2).

Venn diagrams were created from the DEGs described above. GO analysis was performed using barley gene-to-GO associations captured by a Python script from *Arabidopsis* GO annotations (<http://www.arabidopsis.org/download/index.jsp>). The R package clusterProfiler was applied to GO enrichment analysis for DEGs³⁰. The Benjamini–Yekutieli method was used for multitest adjustment to

correct the *P* values. AgriGO2 (<http://systemsbiology.cau.edu.cn/agriGOv2/>) was used for the GO classification analysis and the identification of pathways of stage-specific genes⁶⁰. A corrected false discovery rate of <0.05 was considered to be significantly enriched. REVIGO was applied to summarize and visualize the GO term results as treemaps (Supplementary Datasets 3 and 4)⁷¹. Using SimRel semantic similarity measures, terms were clustered at a specified similarity cut-off and were further manually modified to clarify the meanings of representative terms at low- and high-temperature conditions⁷¹. Genes related to temperature response, meristem transition and development, phytohormone pathways, cell cycle and cell division from DEGs for hierarchical clustering analysis were selected manually (Supplementary Dataset 5) and performed using R⁶⁸.

ChIP-PCR. W3.5 inflorescences (~1 g) from *pro:HvMADS1-eGFP* plants grown at 15 °C/10 °C and 25 °C/20 °C were collected and fixed in buffer (10 mM Tris–HCl, pH 8, 0.4 M sucrose, 0.1 mM phenylmethanesulfonyl fluoride, 5 mM β -mercaptoethanol, 1% (v/v) formaldehyde) under vacuum for 15 min. Fixation was stopped by adding glycine to a final concentration of 125 mM for 5 min under vacuum. The samples were washed and frozen in liquid nitrogen. The ChIP experiments were performed as previously described⁷², with modifications. Briefly, each sample was ground and resuspended in lysis buffer (50 mM HEPES, pH 7.5, 150 mM NaCl, 1 mM EDTA, 1% (v/v) Triton X-100, 0.1% (w/v) deoxycholate, 0.1% (w/v) SDS, 1 mM PMSF, 10 mM sodium butyrate, 1 $\mu\text{g ml}^{-1}$ aprotinin, 1 $\mu\text{g ml}^{-1}$ pepstatin A) to extract the nuclei. DNA was sheared into ~250–750 bp fragments by sonication. After centrifugation (20 min at 13,000 r.p.m.), the supernatants were precleared with 60 μl of salmon sperm (SS) DNA/Protein A agarose (Thermo Fisher Scientific) for 1 h at 4 °C. After 2 min of centrifugation at 1,000 r.p.m., the supernatant was transferred to a siliconized tube, to which was added 10 μl of the anti-eGFP antibody (ABclonal). After shaking incubation overnight at 4 °C, 60 μl of SS DNA/Protein A agarose was added, and incubation continued for 2 h. The agarose beads were collected and washed, as previously described⁷³. The immunocomplexes were eluted from the beads with elution buffer (1% (w/v) SDS, 0.1 M NaHCO₃). Sodium chloride was added to a final concentration of 0.2 M, and crosslinks were reversed by incubation at 65 °C overnight. Residual protein was degraded by the addition of 20 μg of Proteinase K in 10 mM EDTA and 40 mM Tris, pH 8, at 45 °C for 1 h, followed by phenol/chloroform/isoamyl alcohol extraction and ethanol precipitation. The pellets were resuspended in 50 μl of 1× TE. DNA was diluted 1:5, and approximately 1–2 μl was used for qPCR in a 384-well QuantStudio Flex 6 (Thermo Fisher Scientific) machine. Each immunoprecipitation was performed at least three times, and control precipitations without antibodies were conducted at the same time. PCR was done as six independent replicates, with the final relative values calculated by normalizing against the fraction of input. The HvACT7 gene, which is not an HvMADS1 target gene, was used as a negative control. All primers are listed in Supplementary Table 6.

Dual-luciferase assays. The dual-luciferase method was modified from a previously described protocol using *N. benthamiana* plants⁶². Effector plasmids were prepared by cloning full-length cDNAs of HvMADS1 and HvMADS3 into the *Hind*III–*Bam*HI site of the pGreenII-0000 vector that contains the 35S promoter. Full-length HvCKX3 promoter (*proHvCKX3*) and truncated *proHvCKX3ΔI-ΔVI* promoters (Extended Data Fig. 10f) were amplified from the barley genome and cloned upstream of the *LUC* reporter gene in pGreenII-0800–LUC using the *Hind*III site via an infusion kit (Clontech). Two CArG-box promoters fused to the minimum 35S promoter were synthesized by Generay Biotech: *proCArG-wt* contained three wild-type A-tract boxes, and *proCArG-mu* had its A-tract CArG-boxes replaced by non-A-tract CArG-boxes. These promoters were cloned into the *Hind*III–*Bam*HI site of pUC19 and then recombined into the binary vector pGreenII-0800–LUC. The sequences of the recombinant CArG-box promoters are included in Supplementary Data 1. The primer sequences for all of the constructs are listed in Supplementary Table 7. All effectors (including empty vector, pGreenII-0000) and reporter constructs were transformed into *A. tumefaciens* GV3101 cells containing the helper plasmid pSoup-P19, which encodes a repressor of co-suppression.

Overnight *Agrobacterium* cultures were collected and resuspended, as previously described⁶². The reporter strain was incubated either with empty vector or as a mixture with the effector strain (at a reporter:effector ratio of 1:4). The mixture was infiltrated into a young *N. benthamiana* leaf, and the plants were grown for about 48 h. Leaf samples were collected for the dual-luciferase assay using commercial reagents, according to the manufacturer's instructions (Promega). LUC was quenched and the REN reaction initiated by the addition of 100 μl of Stop and Glow buffer (Promega), using a refurbished GloMax-96 Microplate Luminometer (Promega). At least five biological repeats were measured for each sample. The LUC/REN activity obtained from a co-transfection with an empty effector and reporter construct was set to one for normalization.

EMSA. Selected promoter regions of HvCKX3 were amplified by PCR from barley genomic DNA, and artificial CArG-wt/mu oligonucleotides were amplified by PCR from dual-luciferase reporter vectors as mentioned above, using specific primer pairs combined with a universal sequence (5'-AGCCAGTGGCGATAAG-3'). DNA fragments were purified by a DNA purification kit (Thermo Fisher Scientific) and

labelled via PCR using the universal primer sequence containing Cy5 at the 5' end (Generay Biotech). The PCR conditions for Cy5 labelling were 94 °C for 3 min; 35 cycles of 94 °C for 25 s, 55 °C for 25 s and 72 °C for 30 s; and an extension at 72 °C for 5 min.

The coding sequence of HvMADS1 was fused with a T7 promoter sequence (5'-TAATACGACTCACTATAGG-3') by PCR, which was used for protein translation. Proteins were synthesized using the TNT T7 Quick Coupled Transcription/Translation System (Promega) according to the manufacturer's instructions in total volume of 10 µl. The binding reaction mixture was prepared as described previously⁷⁴ and contained 1.2 mM EDTA, pH 8.0; 0.25 mg ml⁻¹ BSA; 7.2 mM HEPES, pH 7.3; 0.7 mM DTT; 60 µg ml⁻¹ SS DNA; 1.3 mM spermidine; 2.5% (v/v) CHAPS; 8% (v/v) glycerol; 5 nmol ml⁻¹ Cy5-labelled DNA; and 3 µl of in vitro synthesized protein. Protein–DNA binding was performed at 4 °C, 15 °C, 25 °C and 30 °C for 30 min before loading on a 5% polyacrylamide gel. Electrophoresis was performed at low voltage (75 V per 6.8 cm gel) to avoid temperature changes. The DNA bands were visualized by fluorescence imaging using the Cy5 channel of the ChemiDoc MP imaging system (Bio-Rad). All primers used for EMSA are listed in Supplementary Table 8.

Co-immunoprecipitation. Co-immunoprecipitation analysis was performed with extracts from four-week-old tobacco leaves, as previously described⁶². To create the Flag-tagged and HA-tagged HvMADS1 constructs for in vivo protein expression, the full-length coding region of HvMADS1 fused with 3× Flag tag or 6× HA tag was cloned into the *HindIII-BamHI* site of the pGreenII-0000 vector that contains the 35S promoter (the primers are listed in Supplementary Table 9). The fusion proteins HvMADS1-Flag and HvMADS1-HA were transiently expressed in tobacco leaves as described above ('Dual-luciferase assays'). The proteins were extracted with ice-cold buffer containing 20 mM HEPES-KOH at pH 7.5, 40 mM KCl, 1 mM EDTA, 1% (v/v) Triton X-100, 1 mM PMSF, 10 mM sodium butyrate, 1 µg ml⁻¹ aprotinin and 1 µg ml⁻¹ pepstatin A. After centrifugation at 16,000 r.p.m. for 10 min, the supernatant was incubated with anti-HA antibody (Abcam; catalogue number, ab13783) and IgG-bound to Protein A Sepharose beads (Thermo Fisher Scientific) for 2 h at 4 °C, and the beads were washed five times with wash buffer (20 mM HEPES-KOH at pH 7.5, 40 mM KCl, 0.1% (v/v) Triton X-100). The proteins were eluted by boiling the beads in 2× SDS sample buffer and separated on SDS-PAGE before immunoblotting using anti-Flag (1:1,000 dilution; ThermoFisher; catalogue number, MA1-91878) or anti-HA (1:1,000 dilution) antibodies.

CK treatment and endogenous CK measurement. CK treatments of barley inflorescence were performed using a modified method as previously described³⁹. Wild-type and *Hvmads1* plants grown at low and high temperatures were injected with 0 mM (mock), 1 mM and 5 mM BAP (Sigma). The treatments were applied every two days starting from spike stage W1 (two- to three-leaf stage) and stopped at stage W5 (six-leaf stage)³⁵.

For endogenous CK level measurement, three replicates of 200–300 mg of W3.5 spikes were collected from wild-type and *Hvmads1* plants grown at low and high temperatures. CKs were extracted and measured as previously described^{75,76}. Briefly, fresh plant tissues were frozen in liquid nitrogen and homogenized to fine powder using a ball mill Retsch MM 400 (Retsch) at a frequency of 30 Hz for 1 min. The powder was extracted for 24 h in solvent (15:4:4 methanol:water:formic acid, v/v/v) with 400 pg of internal standards (IP, iPR, IP9G, tZ, tZR, tZ9G and tZOG). The crude extracts were further purified by loading onto the Oasis MCX cartridge (500 mg per 6 ml; Waters) preconditioned with solvent. The cartridge was sequentially washed with formic acid/methanol solution. Fractions containing CK nucleobases, nucleosides and glucosides were eluted using ammonia/methanol solutions and analysed on a liquid chromatography–tandem mass spectrometer comprising an Acquity UPLC (Waters) and Qtrap 5500 system (AB Sciex) equipped with an electrospray ionization source as described in ref. ⁷⁵. All active CKs, nucleobases, nucleosides and glucosides were measured at the Institute of Genetics and Developmental Biology, Chinese Academy of Sciences. Endogenous concentrations of CK were calculated as previously described⁷⁶.

Variation of HvMADS1. For SNP analysis of HvMADS1, the exome-sequencing data of 276 barley varieties were analysed (<https://www.ebi.ac.uk/ena/data/view/PRJEB8044>)⁵⁰. Morex_contig_202661 containing the HvMADS1 gene was used for SNP investigation compared with the reference genome (Supplementary Dataset 6)⁵⁴. SNP calling was performed manually by visual inspection of the sequences. 101 barley varieties with diverse inflorescence architectures (Supplementary Dataset 7) were grown in a growth chamber. The coding region from the first intron of HvMADS1 were amplified from spike cDNA and genomic DNA by PCR using a Phire Plant Direct PCR Kit (Thermo Fisher Scientific) and sequenced by Sanger sequencing (AGRIF). All primers used for HvMADS1 SNP sequencing are listed in Supplementary Table 10.

Quantification and statistical analysis. All experiments were conducted with technical and biological replicates at appropriate sample sizes estimated on the basis of our previous experience. No statistical methods were used to predetermine sample size. The experiments were not randomized, and the investigators were not blinded to allocation during the experiments and outcome assessment.

For the quantification of EMSA band intensity, multiple exposures of the Cy5 channel with different times were performed to avoid signal saturation, and a mildly exposed image was always selected for signal quantification with ImageJ (version 1.53a; <https://imagej.nih.gov/ij/notes.html>). A constant-sized rectangle was drawn in ImageJ to enclose the band, and the intensity inside it was measured. For each gel lane, the measured values were normalized to the average intensity of all the measurements to remove systematic variability.

All experiments were replicated independently at least once, as indicated in each figure. Dot plots were routinely used to show individual data points for each experimental observation, and the bar graphs contain individual data points for each experimental replicate. Statistical analyses of all box plots and bar graphs were performed using GraphPad Prism 8.0.2 (<https://www.graphpad.com/scientific-software/prism/>) or Microsoft Excel 2016. One-way or two-way ANOVA was used to evaluate significant variations between genotypes or temperatures, as appropriate, using GraphPad Prism 8. Tukey's post-hoc test was used to assess the statistical difference in comparisons after a one-way or two-way ANOVA. Values of $P < 0.05$ were considered statistically significant. The details about the statistical approaches used can be found in the figures or figure legends. The data are presented as mean \pm s.d.

Reporting Summary. Further information on research design is available in the Nature Research Reporting Summary linked to this article.

Data availability

The raw data files for the RNA-seq analysis reported in this paper have been deposited in the GEO database (accession no. [GSE156526](https://www.ncbi.nlm.nih.gov/geo/study/GSE156526)). The data supporting the findings of this study are available within the paper and its Supplementary Information files. Source data are provided with this paper. Additional data, such as raw image files, that support the findings of this study are available from the corresponding author upon request.

Received: 10 September 2020; Accepted: 2 June 2021;

Published online: 28 June 2021

References

- Franks, S. J., Sim, S. & Weis, A. E. Rapid evolution of flowering time by an annual plant in response to a climate fluctuation. *Proc. Natl Acad. Sci. USA* **104**, 1278–1282 (2007).
- Nicotra, A. B. et al. Plant phenotypic plasticity in a changing climate. *Trends Plant Sci.* **15**, 684–692 (2010).
- Scheepens, J. F., Deng, Y. & Bossdorf, O. Phenotypic plasticity in response to temperature fluctuations is genetically variable, and relates to climatic variability of origin, in *Arabidopsis thaliana*. *AoB Plants* **10**, ply043 (2018).
- Casal, J. J. & Balasubramanian, S. Thermomorphogenesis. *Annu. Rev. Plant Biol.* **70**, 321–346 (2019).
- Quint, M. et al. Molecular and genetic control of plant thermomorphogenesis. *Nat. Plants* **2**, 15190 (2016).
- Kumar, S. V. & Wigge, P. A. H2A.Z-containing nucleosomes mediate the thermosensory response in *Arabidopsis*. *Cell* **140**, 136–147 (2010).
- Jung, J. H. et al. Phytochromes function as thermosensors in *Arabidopsis*. *Science* **354**, 886–889 (2016).
- Kumar, S. V. et al. Transcription factor PIF4 controls the thermosensory activation of flowering. *Nature* **484**, 242–245 (2012).
- Bommert, P. & Whipple, C. Grass inflorescence architecture and meristem determinacy. *Semin. Cell Dev. Biol.* **79**, 37–47 (2018).
- Zhang, D. & Yuan, Z. Molecular control of grass inflorescence development. *Annu. Rev. Plant Biol.* **65**, 553–578 (2014).
- Wang, C., Yang, X. & Li, G. Molecular insights into inflorescence meristem specification for yield potential in cereal crops. *Int. J. Mol. Sci.* **22**, 3508 (2021).
- Prusinkiewicz, P., Erasmus, Y., Lane, B., Harder, L. D. & Coen, E. Evolution and development of inflorescence architectures. *Science* **316**, 1452–1456 (2007).
- Jacott, C. N. & Boden, S. A. Feeling the heat: developmental and molecular responses of wheat and barley to high ambient temperatures. *J. Exp. Bot.* **71**, 5740–5751 (2020).
- Urban, M. C. Accelerating extinction risk from climate change. *Science* **348**, 571–573 (2015).
- Preston, J. C. & Fjellheim, S. Understanding past, and predicting future, niche transitions based on grass flowering time variation. *Plant Physiol.* **183**, 822–839 (2020).
- Wahid, A., Gelani, S., Ashraf, M. & Foolad, M. R. Heat tolerance in plants: an overview. *Environ. Exp. Bot.* **61**, 199–223 (2007).
- Lobell, D. B., Schlenker, W. & Costa-Roberts, J. Climate trends and global crop production since 1980. *Science* **333**, 1186–1189 (2011).
- Zhao, C. et al. Temperature increase reduces global yields of major crops in four independent estimates. *Proc. Natl Acad. Sci. USA* **114**, 9326–9331 (2017).
- Pelaz, S., Ditta, G. S., Baumann, E., Wisman, E. & Yanofsky, M. F. B and C floral organ identity functions require SEPALLATA MADS-box genes. *Nature* **405**, 200–203 (2000).

20. Malcomber, S. T. & Kellogg, E. A. *SEPALLATA* gene diversification: brave new whorls. *Trends Plant Sci.* **10**, 427–435 (2005).
21. Liu, C. et al. A conserved genetic pathway determines inflorescence architecture in *Arabidopsis* and rice. *Dev. Cell* **24**, 612–622 (2013).
22. Gao, X. C. et al. The *SEPALLATA*-like gene *OsMADS34* is required for rice inflorescence and spikelet development. *Plant Physiol.* **153**, 728–740 (2010).
23. Soyk, S. et al. Bypassing negative epistasis on yield in tomato imposed by a domestication gene. *Cell* **169**, 1142–1155 (2017).
24. Käppel, S., Melzer, R., Rümpfer, F., Gafert, C. & Theissen, G. The floral homeotic protein *SEPALLATA* 3 recognizes target DNA sequences by shape readout involving a conserved arginine residue in the MADS-domain. *Plant J.* **95**, 341–357 (2018).
25. Muiño, J. M., Smaczniak, C., Angenent, G. C., Kaufmann, K. & van Dijk, A. D. Structural determinants of DNA recognition by plant MADS-domain transcription factors. *Nucleic Acids Res.* **42**, 2138–2146 (2014).
26. Rohs, R. et al. The role of DNA shape in protein-DNA recognition. *Nature* **461**, 1248–1253 (2009).
27. Prosseda, G. et al. A temperature-induced narrow DNA curvature range sustains the maximum activity of a bacterial promoter in vitro. *Biochemistry* **49**, 2778–2785 (2010).
28. Huang, Q., Duan, B., Dong, X., Fan, S. & Xia, B. GapR binds DNA through dynamic opening of its tetrameric interface. *Nucleic Acids Res.* **48**, 9372–9386 (2020).
29. Callens, C., Tucker, M. R., Zhang, D. & Wilson, Z. A. Dissecting the role of MADS-box genes in monocot floral development and diversity. *J. Exp. Bot.* **69**, 2435–2459 (2018).
30. Liu, H. et al. Transcriptome profiling reveals phase-specific gene expression in the developing barley inflorescence. *Crop J.* **8**, 71–86 (2020).
31. Ma, X. et al. A robust CRISPR/Cas9 system for convenient, high-efficiency multiplex genome editing in monocot and dicot plants. *Mol. Plant* **8**, 1274–1284 (2015).
32. Poursarebani, N. et al. COMPOSITUM 1 contributes to the architectural simplification of barley inflorescence via meristem identity signals. *Nat. Commun.* **11**, 5138 (2020).
33. Poursarebani, N. et al. The genetic basis of composite spike form in barley and ‘Miracle-Wheat’. *Genetics* **201**, 155–165 (2015).
34. Koppolu, R. et al. *Six-rowed spike4* (*Vrs4*) controls spikelet determinacy and row-type in barley. *Proc. Natl Acad. Sci. USA* **110**, 13198–13203 (2013).
35. Waddington, S. R., Cartwright, P. M. & Wall, P. C. A quantitative scale of spike initial and pistil development in barley and wheat. *Ann. Bot.* **51**, 119–130 (1983).
36. Ramsay, L. et al. *INTERMEDIUM-C*, a modifier of lateral spikelet fertility in barley, is an ortholog of the maize domestication gene *TEOSINTE BRANCHED 1*. *Nat. Genet.* **43**, 169–172 (2011).
37. Shang, Y. et al. A CYC/TB1-type TCP transcription factor controls spikelet meristem identity in barley. *J. Exp. Bot.* **71**, 7118–7131 (2020).
38. Komatsuda, T. et al. Six-rowed barley originated from a mutation in a homeodomain-leucine zipper I-class homeobox gene. *Proc. Natl Acad. Sci. USA* **104**, 1424–1429 (2007).
39. Youssef, H. M. et al. VR52 regulates hormone-mediated inflorescence patterning in barley. *Nat. Genet.* **49**, 157–161 (2017).
40. Bull, H. et al. Barley *SIX-ROWED SPIKE3* encodes a putative Jumonji C-type H3K9me2/me3 demethylase that represses lateral spikelet fertility. *Nat. Commun.* **8**, 936 (2017).
41. Chuck, G., Muszynski, M., Kellogg, E., Hake, S. & Schmidt, R. J. The control of spikelet meristem identity by the *branched silkless1* gene in maize. *Science* **298**, 1238–1241 (2002).
42. Komatsu, M., Chujo, A., Nagato, Y., Shimamoto, K. & Kyozuka, J. *FRIZZY PANICLE* is required to prevent the formation of axillary meristems and to establish floral meristem identity in rice spikelets. *Development* **130**, 3841–3850 (2003).
43. Satoh-Nagashawa, N., Nagashawa, N., Malcomber, S., Sakai, H. & Jackson, D. A trehalose metabolic enzyme controls inflorescence architecture in maize. *Nature* **441**, 227–230 (2006).
44. Menges, M., De Jager, S. M., Grussem, W. & Murray, J. A. Global analysis of the core cell cycle regulators of *Arabidopsis* identifies novel genes, reveals multiple and highly specific profiles of expression and provides a coherent model for plant cell cycle control. *Plant J.* **41**, 546–566 (2005).
45. Li, X. M. et al. Natural alleles of a proteasome α 2 subunit gene contribute to thermotolerance and adaptation of African rice. *Nat. Genet.* **47**, 827–833 (2015).
46. Shen, H. et al. Overexpression of receptor-like kinase *ERECTA* improves thermotolerance in rice and tomato. *Nat. Biotechnol.* **33**, 996–1003 (2015).
47. Werner, T. & Schmülling, T. Cytokinin action in plant development. *Curr. Opin. Plant Biol.* **12**, 527–538 (2009).
48. Ashikari, M. et al. Cytokinin oxidase regulates rice grain production. *Science* **309**, 741–745 (2005).
49. Han, Y., Zhang, C., Yang, H. & Jiao, Y. Cytokinin pathway mediates APETALA1 function in the establishment of determinate floral meristems in *Arabidopsis*. *Proc. Natl Acad. Sci. USA* **111**, 6840–6845 (2014).
50. Russell, J. et al. Exome sequencing of geographically diverse barley landraces and wild relatives gives insights into environmental adaptation. *Nat. Genet.* **48**, 1024–1030 (2016).
51. Jeon, J. S. et al. *leafy hull sterile1* is a homeotic mutation in a rice MADS box gene affecting rice flower development. *Plant Cell* **12**, 871–884 (2000).
52. Wu, D. et al. Loss of *LOFSEP* transcription factor function converts spikelet to leaf-like structures in rice. *Plant Physiol.* **176**, 1646–1664 (2018).
53. Cui, R. et al. Functional conservation and diversification of class E floral homeotic genes in rice (*Oryza sativa*). *Plant J.* **61**, 767–781 (2010).
54. Mascher, M. et al. A chromosome conformation capture ordered sequence of the barley genome. *Nature* **544**, 427–433 (2017).
55. Harwood, W. A. et al. in *Transgenic Wheat, Barley and Oats* (eds Jones, H. & Shewry, P.) 137–147 (Humana, 2009).
56. Zürcher, E. et al. A robust and sensitive synthetic sensor to monitor the transcriptional output of the cytokinin signaling network in planta. *Plant Physiol.* **161**, 1066–1075 (2013).
57. Curtis, M. D. & Grossniklaus, U. A gateway cloning vector set for high-throughput functional analysis of genes in planta. *Plant Physiol.* **133**, 462–469 (2003).
58. Lim, W. L. et al. Overexpression of *HvCslF6* in barley grain alters carbohydrate partitioning plus transfer tissue and endosperm development. *J. Exp. Bot.* **71**, 138–153 (2020).
59. Heisler, M. G. & Ohno, C. in *Flower Development* (eds Riechmann, J. & Wellmer, F.) 431–440 (Humana, 2014).
60. Kotogány, E., Dudits, D., Horváth, G. V. & Ayaydin, F. A rapid and robust assay for detection of S-phase cell cycle progression in plant cells and tissues by using ethynyl deoxyuridine. *Plant Methods* **6**, 5 (2010).
61. Xiong, Y. et al. Glucose-TOR signalling reprograms the transcriptome and activates meristems. *Nature* **496**, 181–186 (2013).
62. Li, G. et al. Rice actin-binding protein RMD is a key link in the auxin–actin regulatory loop that controls cell growth. *Proc. Natl Acad. Sci. USA* **111**, 10377–10382 (2014).
63. Yang, X. et al. A rice glutamyl-tRNA synthetase modulates early anther cell division and patterning. *Plant Physiol.* **177**, 728–744 (2018).
64. Andrews, S. FastQC: a quality control tool for high throughput sequence data. (*Babraham Bioinformatics*, 2010).
65. Bolger, A. M., Lohse, M. & Usadel, B. Trimmomatic: a flexible trimmer for Illumina sequence data. *Bioinformatics* **30**, 2114–2120 (2014).
66. Pertea, M., Kim, D., Pertea, G. M., Leek, J. T. & Salzberg, S. L. Transcript-level expression analysis of RNA-seq experiments with HISAT, StringTie and Ballgown. *Nat. Protoc.* **11**, 1650–1667 (2016).
67. Anders, S., Pyl, P. T. & Huber, W. HTSeq—a Python framework to work with high-throughput sequencing data. *Bioinformatics* **31**, 166–169 (2015).
68. R Development Core Team. R: A language and environment for statistical computing (*R Foundation for Statistical Computing*, 2017); <http://www.R-project.org/>
69. Love, M. I., Huber, W. & Anders, S. Moderated estimation of fold change and dispersion for RNA-seq data with DESeq2. *Genome Biol.* **15**, 550 (2014).
70. Rau, A. & Maguis-Rabusseau, C. Transformation and model choice for RNA-seq co-expression analysis. *Brief. Bioinform.* **19**, 425–436 (2017).
71. Supek, F., Bošnjak, M., Škunca, N. & Šmuc, T. REVIGO summarizes and visualizes long lists of gene ontology terms. *PLoS ONE* **6**, e21800 (2011).
72. Desvoyes, B., Vergara, Z., Sequeira-Mendes, J., Madeira, S. & Gutierrez, C. in *Plant Chromatin Dynamics* (eds Bemer, M. & Baroux, C.) 71–82 (Humana, 2018).
73. Bowler, C. et al. Chromatin techniques for plant cells. *Plant J.* **39**, 776–789 (2004).
74. Smaczniak, C. et al. Characterization of MADS-domain transcription factor complexes in *Arabidopsis* flower development. *Proc. Natl Acad. Sci. USA* **109**, 1560–1565 (2012).
75. Du, Y. et al. *UNBRANCHED3* regulates branching by modulating cytokinin biosynthesis and signaling in maize and rice. *New Phytol.* **214**, 721–733 (2017).
76. Kojima, M. et al. Highly sensitive and high-throughput analysis of plant hormones using MS-probe modification and liquid chromatography–tandem mass spectrometry: an application for hormone profiling in *Oryza sativa*. *Plant Cell Physiol.* **50**, 1201–1214 (2009).

Acknowledgements

We thank L. Dreni (Instituto de Biología Molecular y Celular de Plantas, Spain), M. Kater (University of Milan, Italy) and M. Bennett (University of Nottingham, UK) for the discussion on the Australian Research Council Discovery Project (grant no. DP170103352 to D.Z. and R.A.B.) and Y. Liu (South China Agricultural University) for providing vectors pYLsgRNA-OsU6a, pYLsgRNA-OsU6b and pYLCRISPR-Cas9_{P_{dBi}}-H for CRISPR–Cas9 editing. We thank J. Chu (Institute of Genetics and Developmental Biology, Chinese Academy of Sciences, Beijing, China) for help with the CK measurements, G. Mayo (Adelaide Microscopy) for assistance in the microscopy work, D. Peet (University of Adelaide) for guidance with dual-luciferase measurement, A. Chieng and H. Zhou (University of Adelaide) for managing the plant materials, and G. Coupland (Max Planck Institute for Plant Breeding Research, Germany),

E. A. Kellogg (Donald Danforth Plant Science Center, USA), D. Smyth (Monash University, Australia), C. Beveridge (University of Queensland, Australia), M. Byrne (University of Sydney, Australia) and S. Boden (University of Adelaide, Australia) for comments on the manuscript. This work was financially supported by the Australian Research Council (grant no. DP170103352 to D.Z. and R.A.B.); an Australia–China Science and Research Fund Joint Research Centres grant (no. ACSRF48187) to D.Z. and G.L.; the Waite Research Institute (WRI) of the University of Adelaide; the National Key Technologies Research and Development Program of China, Ministry of Science and Technology (grant nos. 2016YFD0100804 and 2016YFE0101000 to D.Z.); the National Natural Science Foundation of China (grant nos. 31970803 and 31861163002 to D.Z.) and the Science and Research grant of Southwest University of Science and Technology (no. 19zx7146 to G.L.).

Author contributions

D.Z. and R.A.B. initiated the project. G.L. and D.Z. conceived the project and designed the experiments. G.L. carried out most of the molecular and regulatory experiments. G.L. and H.N.J.K. created the barley *sepallata* mutant lines. H.N.J.K. and X.Y. conducted the scanning electron microscopy work, EdU labelling and RNA *in situ* hybridization. X.Y. carried out the *pro:HvMADS1-eGFP* transformation. H.L. and J.S. analysed the RNA-seq data under the guidance of G.L. and W.L. X.Y., C.S. and M.R.T. conducted the

CK biosensor line and BAP treatment. G.L., H.N.J.K., X.Y., M.R.T., R.W., R.A.B. and D.Z. analysed the results and discussion. G.L., N.B. and D.Z. wrote the manuscript with input from all authors.

Competing interests

The authors declare no competing interests.

Additional information

Extended data is available for this paper at <https://doi.org/10.1038/s41477-021-00957-3>.

Supplementary information The online version contains supplementary material available at <https://doi.org/10.1038/s41477-021-00957-3>.

Correspondence and requests for materials should be addressed to G.L. or D.Z.

Peer review information *Nature Plants* thanks Maria von Korff, Clinton Whipple and the other, anonymous, reviewer(s) for their contribution to the peer review of this work.

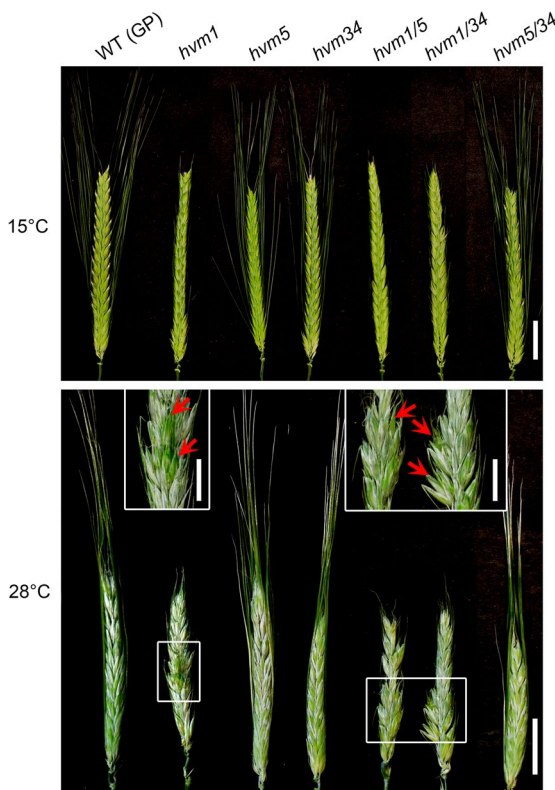
Reprints and permissions information is available at www.nature.com/reprints.

Publisher's note Springer Nature remains neutral with regard to jurisdictional claims in published maps and institutional affiliations.

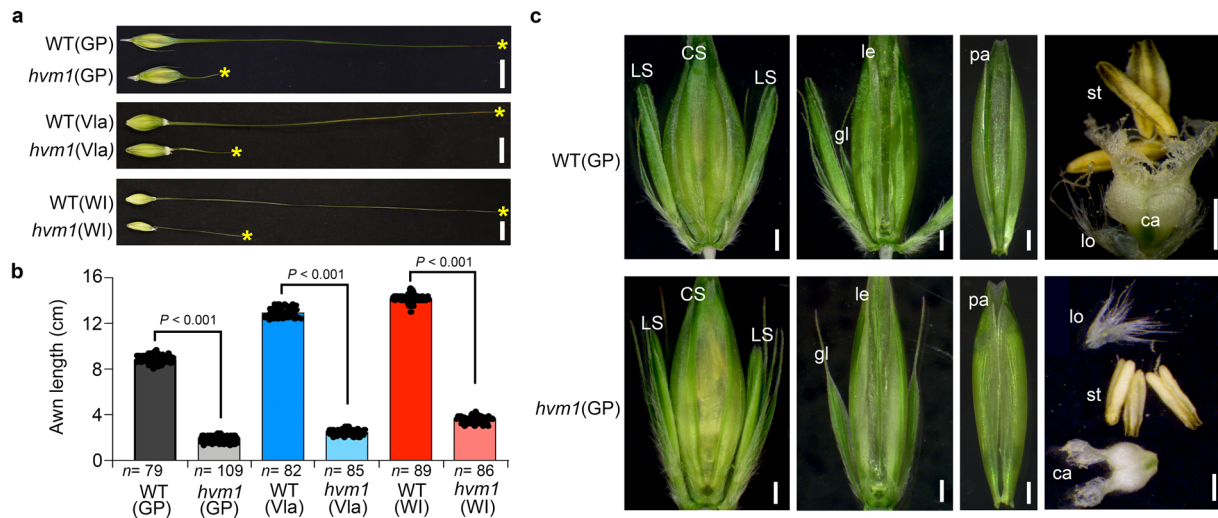
© The Author(s), under exclusive licence to Springer Nature Limited 2021



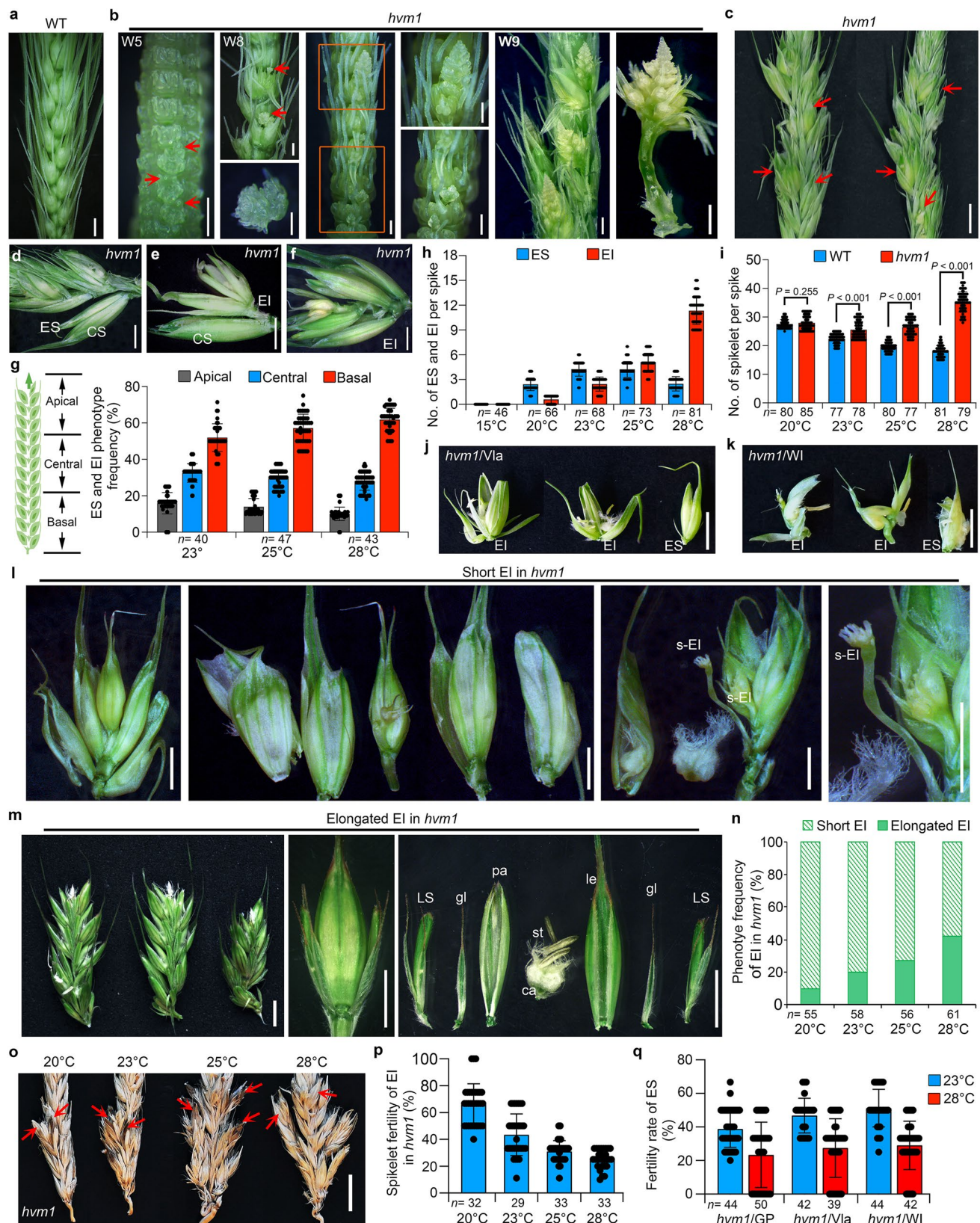
Extended Data Fig. 1 | Creation of barley *sep* mutants using CRISPR-Cas9. **a**, The gene structure of *HvMADS1* and positions of two sgRNA targets (T1 and T2) for CRISPR-Cas9 editing in the MADS-box domain. Blue rectangles indicate exons of *HvMADS1*. **b**, DNA sequences of independent T_0 transgenics of *Hvmads1* (*hvm1*) mutants in GP, WI, and Vla backgrounds, and *hvm1*/5 and *hvm1*/34 double mutants in GP, carrying putative *HvMADS1* biallelic and homozygous mutations. WT, wild-type. **c**, The putative amino acid sequences encoding *HvMADS1* of *hvm1* single mutant, and *hvm1*/5 and *hvm1*/34 double mutants [from (b)]. Asterisks indicate a stop codon. **d,e**, Genotypes of three independent lines of two sgRNA targets of *HvMADS5* (**d**) and *HvMADS34* (**e**) in *hvm5* and *hvm34* single mutants, and *hvm1*/5, *hvm1*/34 and *hvm5*/34 double mutants that were used for CRISPR-Cas9 editing, respectively.



Extended Data Fig. 2 | Spike phenotypes of *sep* single and double mutants under control and heat stress conditions. Images represent spike architecture of barley WT (GP), *hvm1*, *hvm5*, *hvm34* single mutants, and *hvm1/5*, *hvm1/34*, *hvm5/34* double mutants at 15 °C and 28 °C. Red arrows indicate the ectopic organs. Bars = 2 cm, bars in enlarged regions are 1 cm.

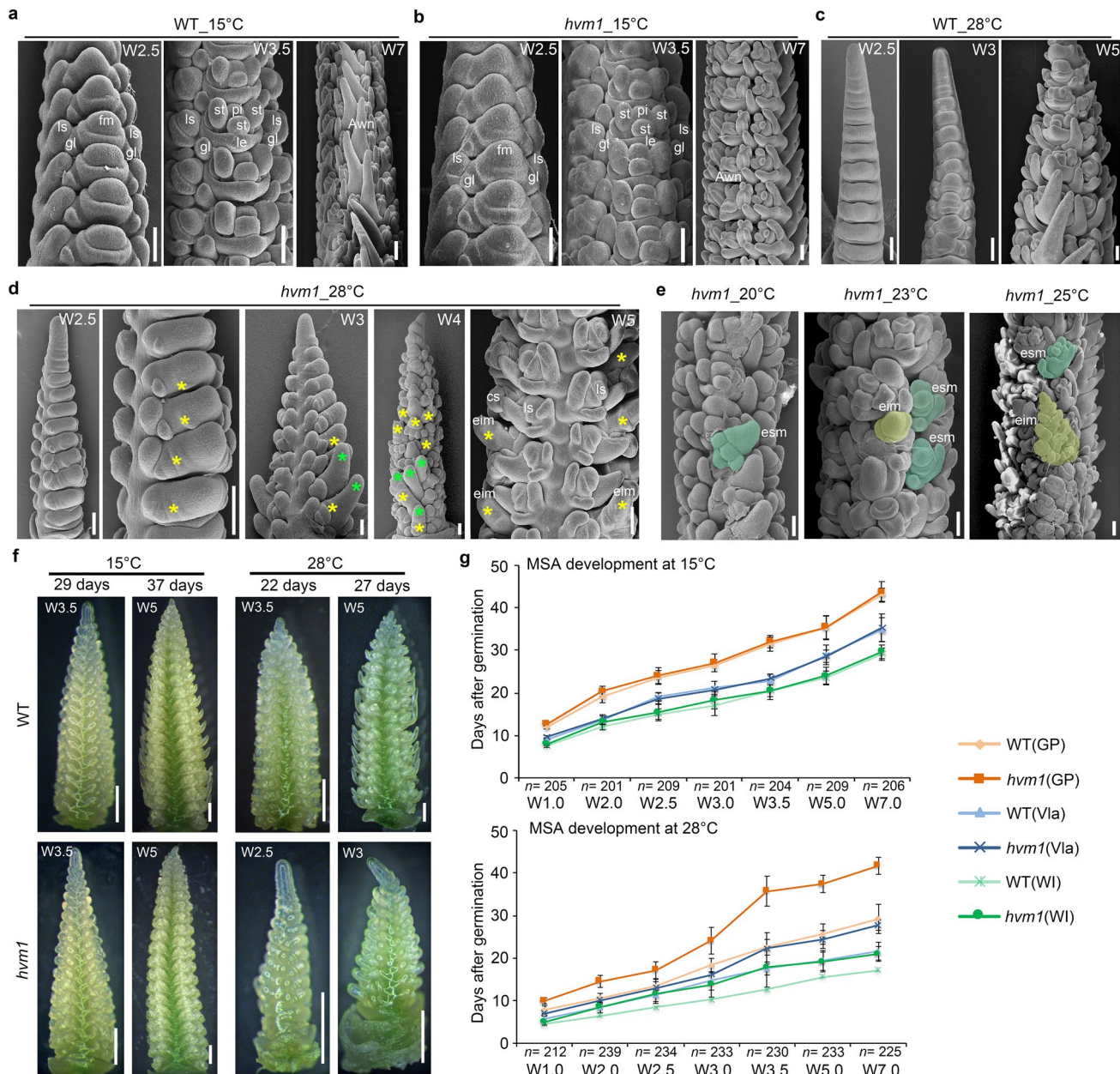


Extended Data Fig. 3 | Spikelet phenotype of *Hvmads1* mutant under normal temperature. **a**, The awn phenotype of *hvm1* central spikelet in GP, Vla and WI backgrounds at 15 °C. Yellow asterisks indicate awn length. Bars = 1 cm. **b**, Average awn length in *hvm1* and WT plants. Data shown as mean \pm s.d. *P* values indicate results from indicated pairwise comparisons of one-way ANOVA tests. **c**, Floret organ (lemma, palea, stamen and pistil) phenotype in the WT (GP) and *hvm1* plants at 15 °C. CS, central spikelet; LS, lateral spikelet; le, lemma; pa, palea; gl, glume; st, stamen; ca, carpel; lo, lodicule. Bars = 1 mm.

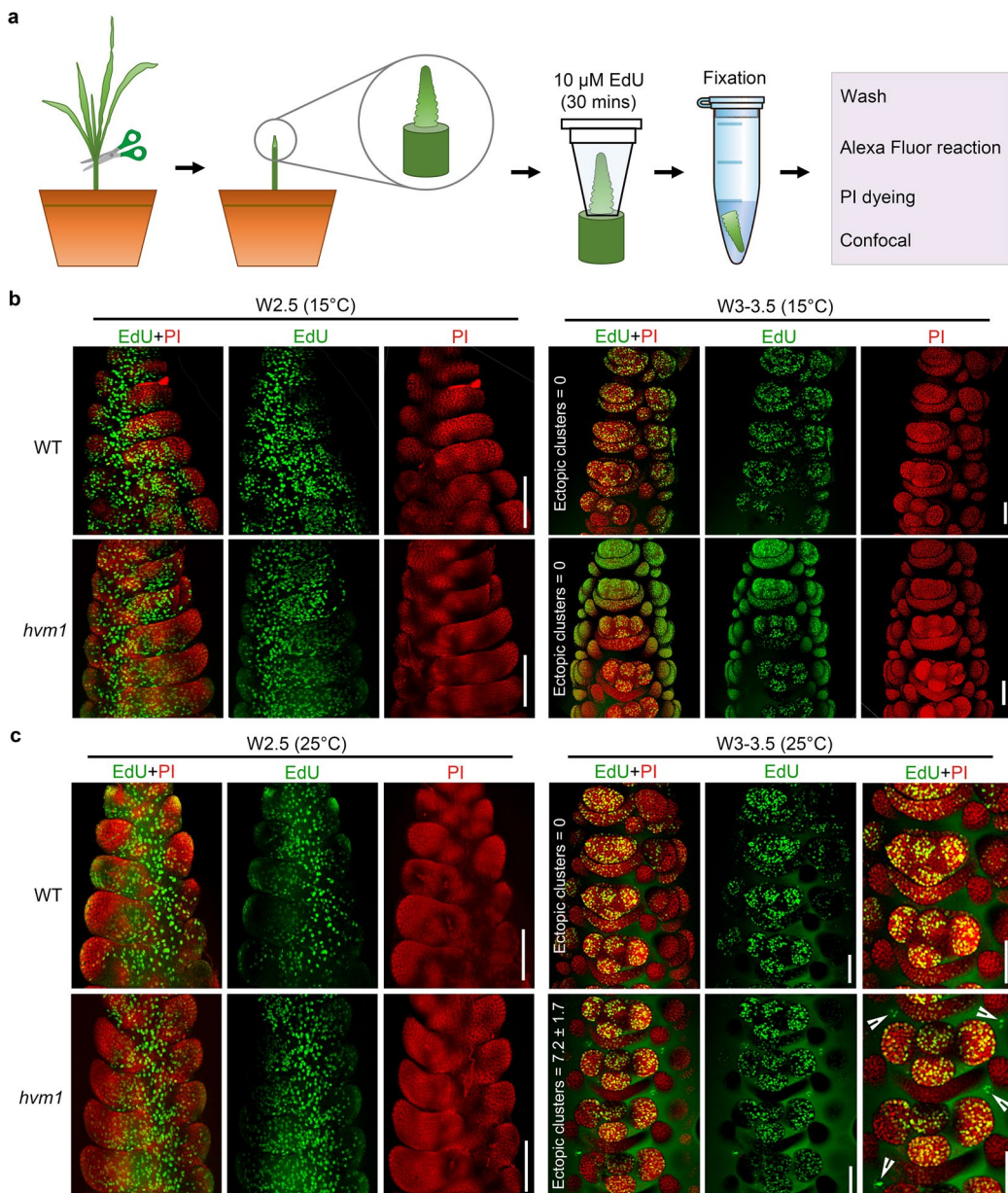


Extended Data Fig. 4 | See next page for caption.

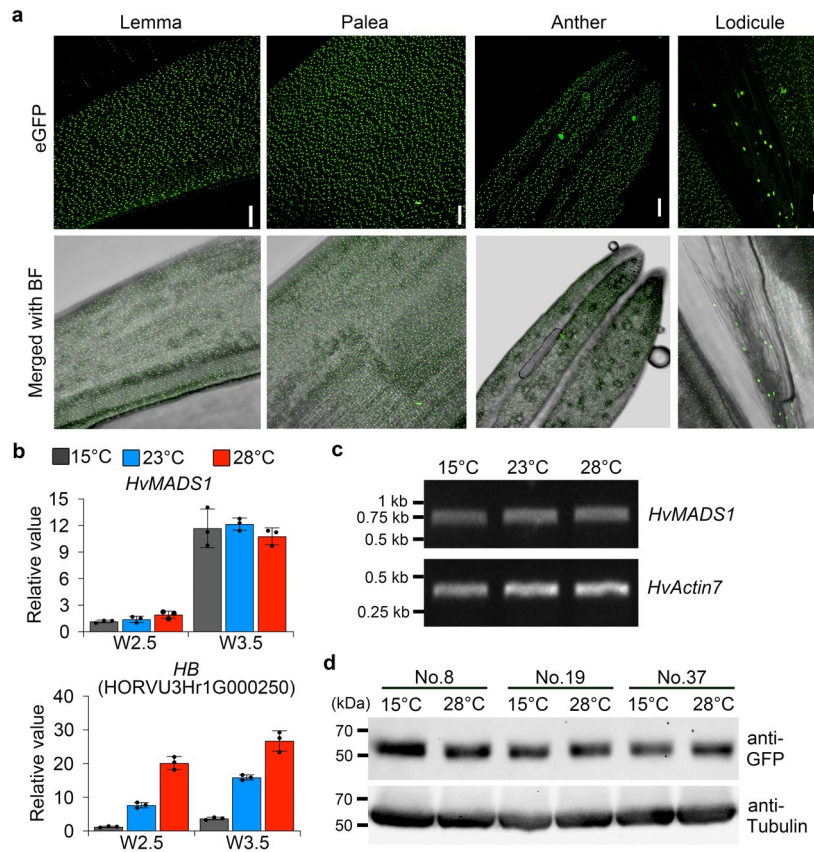
Extended Data Fig. 4 | High ambient temperature induces the production of ectopic organs in *Hvmads1* inflorescences. **a**, WT (GP) inflorescence architecture at W9 at 28 °C. Bar = 0.5 cm. **b**, The developing *hvm1* inflorescence from W5–9 at 28 °C. Red arrows indicate ectopic organs. Bars = 0.5 cm. **c**, The *hvm1* heading spike at 28 °C. Red arrows indicate ectopic organs. Bar = 0.5 cm. **d–f**, The ES (ectopic spikelet) (**d**) and EI (ectopic inflorescence) (**e,f**) of the *hvm1* spike grown at 28 °C. CS, central spikelet. Bars = 0.2 cm. **g**, The frequency of ES and EI in *hvm1* spike sections (basal, central and apical) at different temperatures. Data shown as mean \pm s.d., **h**, The average ES and EI number per *hvm1* spike at five temperature conditions. Data shown as mean \pm s.d. **i**, Total spikelet numbers, including spikelet from ES/EI, per WT or *hvm1* spike at W7 at different temperatures. Data shown as mean \pm s.d. *P* values indicate results from indicated pairwise comparisons of one-way ANOVA tests. **j,k**, The ES and EI induced by high ambient temperatures in *hvm1* mutants of V1a (**j**) and WI (**k**) backgrounds. Bars = 0.5 cm. **l,m**, short (**l**) and elongated (**m**) EI branches with different spikelet morphology. s-EI, secondary EI branch; LS, lateral spikelet; le, lemma; pa, palea; st, stamen; ca, carpel; gl, glume. Bars = 0.5 cm. **n**, The frequency of short and elongated EI phenotype in *hvm1* mutants at different temperatures. **o**, Mature spike of *hvm1* (GP) mutant after treatment at high temperatures. Red arrows indicate fertile spikelets from EI or ES. Bar = 1 cm. **p**, Spikelet fertility rate of EI induced by high temperatures in *hvm1* (GP) spikes. Data shown as mean \pm s.d. **q**, Fertility rate of ES in *hvm1* mutants of three backgrounds at 23 °C and 28 °C. Data shown as mean \pm s.d. All individual biological experiments were repeated at least three times with similar results.



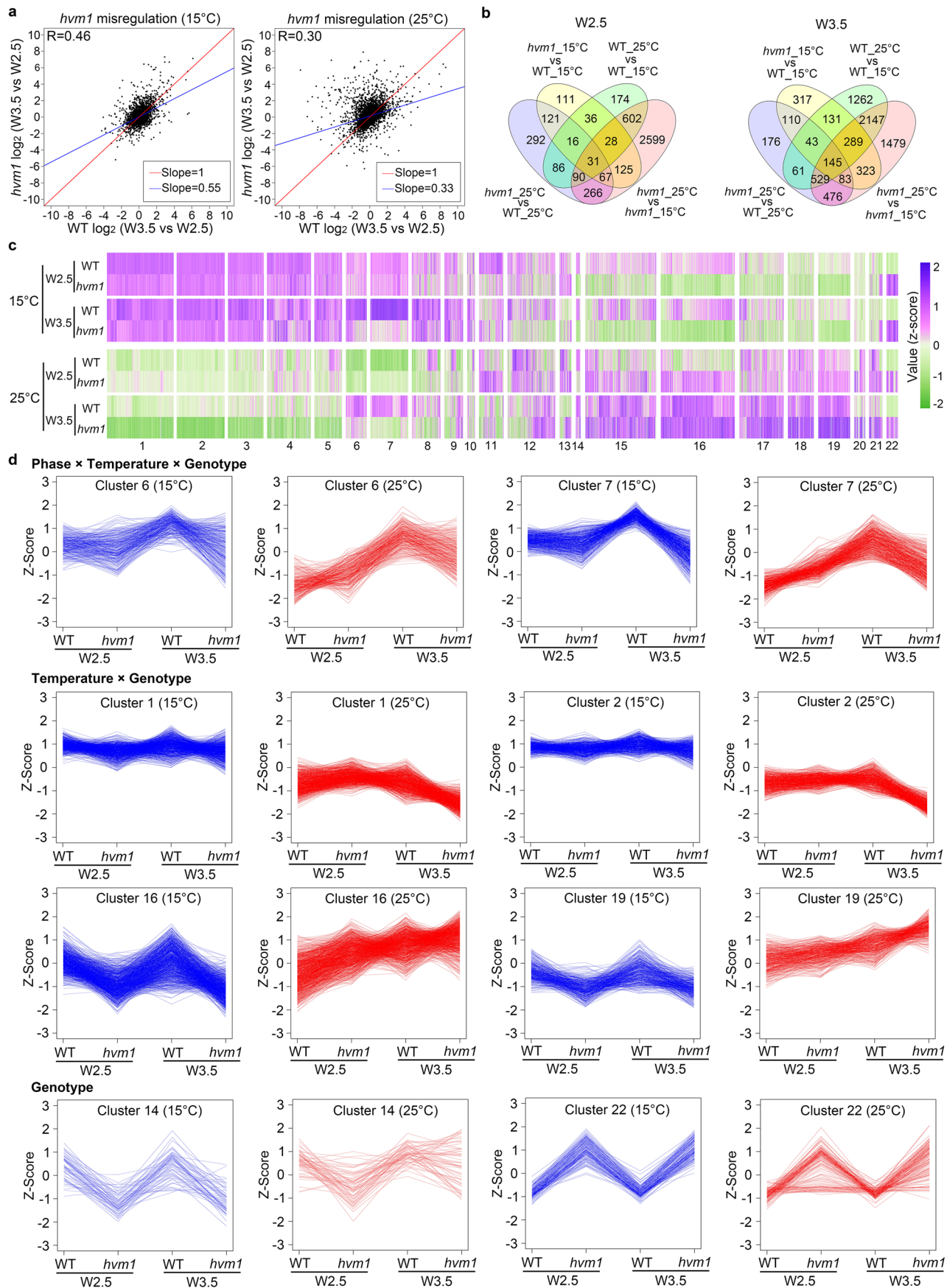
Extended Data Fig. 5 | Loss of Hvmads1 leads to reduced meristem determinacy and delayed inflorescence development under high temperature. **a,b**, Scanning electron microscopy of spike morphology at W2.5, W3.5 and W7 in WT (GP) (**a**) and *hvm1* (**b**) plants at 15 °C, showing the short awn in *hvm1*. **c**, Morphology of the developing WT spike at 28 °C. **d**, Reduced meristem determinacy of *hvm1* inflorescences at 28 °C. Green asterisks indicate the indeterminate inflorescence meristem likely converted from the central spikelet meristems, yellow asterisks indicate the ectopic initiated meristems or inflorescence/spikelet meristems possibly reverted from rachilla. **e**, Effects of ambient high temperatures 20 °C, 23 °C and 25 °C on morphology of *hvm1* spike. Yellow shading indicates EI, blue shading indicates ES. All bars (**a–e**) = 100 µm. fm, floral meristem; ls, lateral spikelet; cs, central spikelet; gl, glume; st, stamen; pi, pistil; le, lemma; esm, ectopic spikelet meristem; eim, ectopic inflorescence meristem. **f**, Rate of spike development at different temperatures, showing delay in *hvm1* (GP) at 28 °C, compared with WT, spike development. Bars = 0.5 mm. **g**, Days to reach different Waddington stages of spike development at 15 °C and 28 °C in three barley varieties and related *hvm1* mutants. Data shown as mean \pm s.d. $P < 0.001$, two-way ANOVA tests of WT and *hvm1* (three background comparisons) at 28 °C. All experiments with treatment were repeated independently at least three times with similar results.



Extended Data Fig. 6 | HvMADS1 represses cell division in the spike in response to high temperature. **a**, Indicative method of EdU (5-ethynyl-2'-deoxyuridine) tracking in barley spike. PI, propidium iodide. **b,c**, EdU tracking of cell division activities in WT (GP) and *hmv1* spikes (W2.5 and W3-3.5) grown at 15 °C (**b**) and 25 °C (**c**). White arrowheads indicate ectopic EdU clusters in non-floret meristem regions of the central spikelet, which shows high levels of cell division activity in ectopic meristems of *hmv1* plants. Numbers of ectopic clusters represent the average observed additional EdU signal clusters in non-floret meristem regions per spike (W3-3.5). Also see the Source Data. Bars = 100 μm . The pictures of EdU tracking assays represent one of three experiments performed independently with similar results.

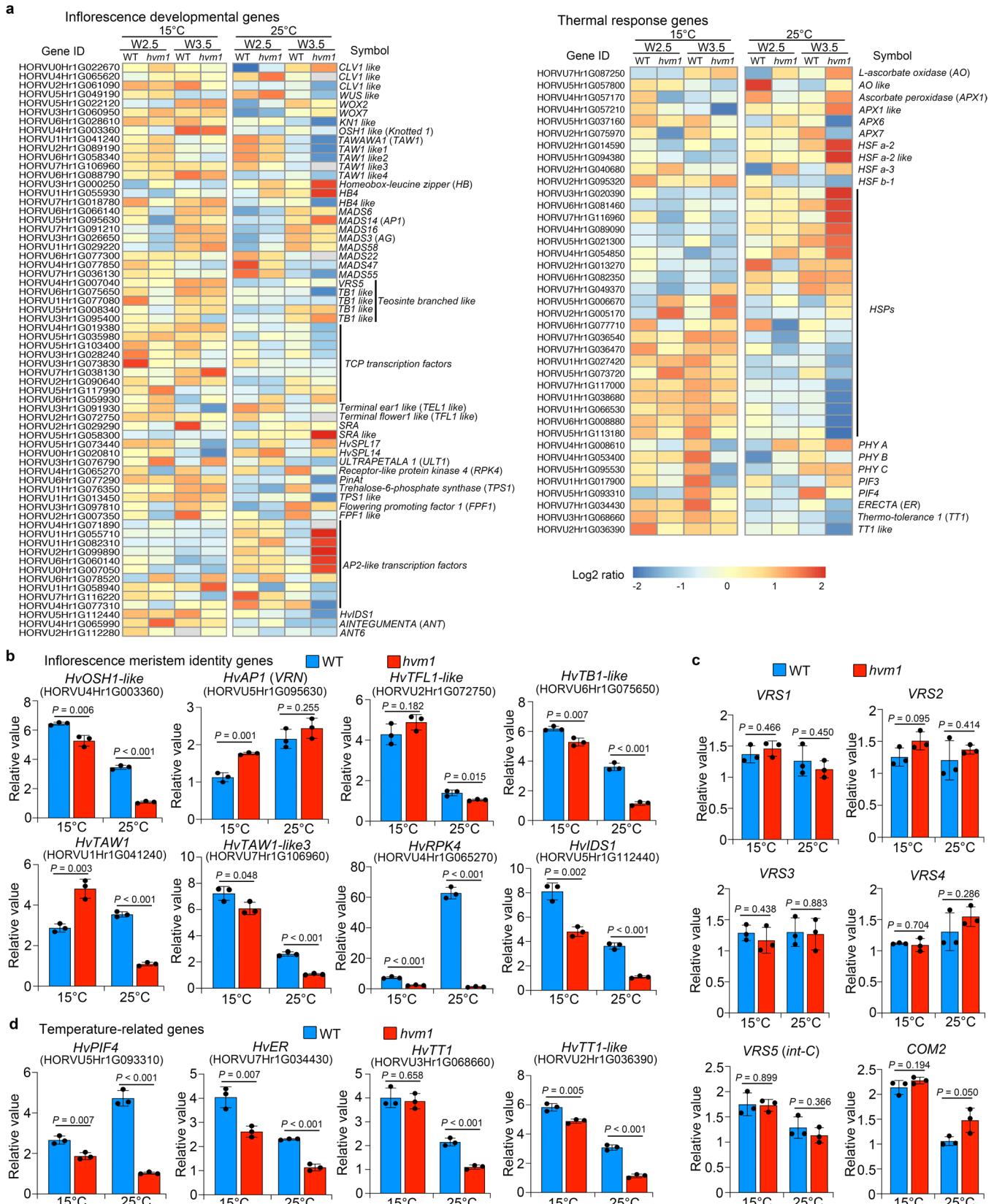


Extended Data Fig. 7 | Temperature does not alter *HvMADS1* mRNA expression or protein accumulation. **a**, Accumulation of the *HvMADS1* protein in flower organs, including lemma, palea, anther, and lodicule, in *pro:HvMADS1-eGFP* transgenic lines at 15 °C. BF, bright field. Bars = 100 µm. **b**, qRT-PCR analysis of *HvMADS1* expression in W2.5 and W3.5 WT spikes at different temperatures. A temperature-responsive gene (*HB*, *homeobox*) served as the positive control. Data shown as mean ± s.d., $n=3$ biological replicates. **c**, RT-PCR analysis of *HvMADS1* expression in WT spikes (W3.5). *HvActin7* served as the control. kb indicates kilobase. **d**, Immunoblot analysis of *HvMADS1-eGFP* protein in W3.5 spikes from three independent *pro:HvMADS1-eGFP* transgenic lines in response to temperatures. Tubulin served as a loading control. All experiments were repeated independently at least three times with similar results.



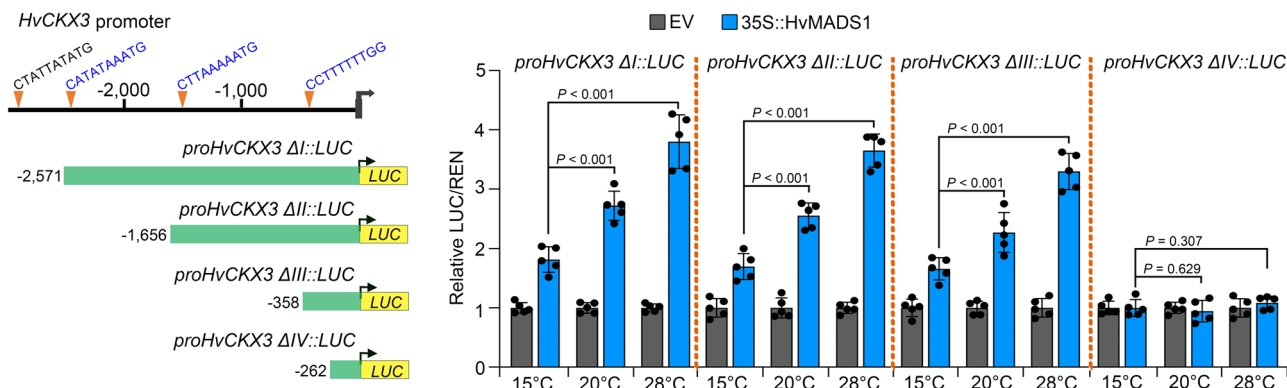
Extended Data Fig. 8 | See next page for caption.

Extended Data Fig. 8 | HvMADS1 regulates the transcriptome of barley inflorescence in response to temperature. **a**, Correlation analysis of transcripts showing mis-regulation of spike developmental genes in *hvm1* plants at 15 °C (left) and, more obviously, at 25 °C (right). **b**, Venn diagram showing the number of DEGs affected by genotype and temperature at two developmental stages. **c**, Co-expression clustering of all DEGs in eight transcriptomes (W2.5 and W3.5 of WT and *hvm1* spikes at 15 °C and 25 °C). Clustering was performed on the expression-filtered data set using a Gaussian mixture model. The number of clusters was assumed to be random and was automatically learned using an empirical Bayes approach (variational Bayesian inference). **d**, DEG clusters in response to temperature, developmental phase and HvMADS1 genotype in inflorescence meristems. Z-score represents variation in gene expression that is likely to be regulated by the interaction between phase × temperature × genotype, temperature × genotype, or only HvMADS1 genotype for selected clusters. Three biological repeats were performed for transcriptome.



Extended Data Fig. 9 | See next page for caption.

Extended Data Fig. 9 | Effects of *Hvmds1* mutation on the expression of key regulators in response to temperature. **a**, Heat map showing DEGs relevant to spike development (left) and temperature response (right). **b**, qRT-PCR analysis of selected genes related to inflorescence meristem identity in W3.5 WT (GP) and *hvm1* spikes at 15 °C and 25 °C. *OSH1*, *ORYZA SATIVA HOMEOBOX1*; *API*, *APETALA 1*; *VRN*, *VERNALIZATION*; *TFL1*, *TERMINAL FLOWER 1*; *TB1*, *TEOSINTE BRANCHED 1*; *TAW1*, *TAWAWA1*; *RPK4*, *RECEPTOR-LIKE PROTEIN KINASE 4*; *IDS1*, *INDETERMINATE SPIKELET 1*. **c**, qRT-PCR analysis of selected genes known to regulate barley spike development, spikelet identity and row-type in W3.5 WT and *hvm1* spikes at 15 °C and 25 °C. *VRS*, *SIX-ROWED SPIKE*; *COM2*, *COMPOSITUM 2*. **d**, qRT-PCR analysis of selected genes related to temperature response in W3.5 WT and *hvm1* spikes at 15 °C and 25 °C. *PIF4*, *PHYTOCHROME-INTERACTING FACTOR 4*; *ER*, *ERECTA*; *TT1*, *THERMO-TOLERANCE 1*. *HvActin7* and *HvEF2* were used for normalisation. For (**b-d**), data shown as mean ± s.d., n=3 biological replicates. P values indicate results from indicated pairwise comparisons of one-way ANOVA tests (**b-d**).



Extended Data Fig. 10 | HvMADS1 promotes the activity of the HvCKX3 promoter in a temperature-dependent manner. Truncated HvCKX3 promoter fragments containing 0, 1, 2 or 3 CArG-boxes were fused to the *LUC* reporter gene, and co-transformed with effector plasmids of EV (empty vector) and 35S::*HvMADS1* into tobacco cells. Normalised LUC/REN activity is shown as mean \pm s.d., $n=5$ biological replicates. P values indicate results from indicated pairwise comparisons of one-way ANOVA tests.

Reporting Summary

Nature Research wishes to improve the reproducibility of the work that we publish. This form provides structure for consistency and transparency in reporting. For further information on Nature Research policies, see our [Editorial Policies](#) and the [Editorial Policy Checklist](#).

Statistics

For all statistical analyses, confirm that the following items are present in the figure legend, table legend, main text, or Methods section.

n/a Confirmed

- The exact sample size (n) for each experimental group/condition, given as a discrete number and unit of measurement
- A statement on whether measurements were taken from distinct samples or whether the same sample was measured repeatedly
- The statistical test(s) used AND whether they are one- or two-sided
Only common tests should be described solely by name; describe more complex techniques in the Methods section.
- A description of all covariates tested
- A description of any assumptions or corrections, such as tests of normality and adjustment for multiple comparisons
- A full description of the statistical parameters including central tendency (e.g. means) or other basic estimates (e.g. regression coefficient) AND variation (e.g. standard deviation) or associated estimates of uncertainty (e.g. confidence intervals)
- For null hypothesis testing, the test statistic (e.g. F , t , r) with confidence intervals, effect sizes, degrees of freedom and P value noted
Give P values as exact values whenever suitable.
- For Bayesian analysis, information on the choice of priors and Markov chain Monte Carlo settings
- For hierarchical and complex designs, identification of the appropriate level for tests and full reporting of outcomes
- Estimates of effect sizes (e.g. Cohen's d , Pearson's r), indicating how they were calculated

Our web collection on [statistics for biologists](#) contains articles on many of the points above.

Software and code

Policy information about [availability of computer code](#)

Data collection

Images from Immuno Blotting, DNA gel, co-immunoprecipitation and EMSA were collected with image Lab (Bio-Rad, version 5.2). Confocal images were collected with NIS-Elements AR (Nikon, version v4.2 & v4.30.01). SEM images were collected with Genesis (Philips, version 4.61). Dual-LUC data were collected with GloMax®-96 Microplate Luminometer (Promega, version 1.9.3); LC-MS/MS data of cytokinin measurement were collected with SCIEX Triple Quad™ (AB Sciex, version 5500).

Data analysis

qRT-PCR and ChIP-PCR assays were analyzed with QuantStudio (Thermo Fisher, version 1.3); ; ImageJ (version 1.53a) was used for gel signal quantification.

For RNA-seq: Raw reads were examined using FastQC (version 0.11.4), and were filtered by Trimmomatic (version 0.38) with default parameter. Then filtered reads were aligned to the barley Morex genome (IPK release) using HISAT2 (version 2.0.0) program. Read counts per kilobase per million (RPKM) was normalised using HTSeq (version 0.11.2, <https://htseq.readthedocs.io/en/master/>). The differential expressed genes were analyzed by DESeq2 (version 3.11). Co-expression clustering were performed using coseq Bioconductor package (version 1.0.1). Gene ontology enrichment was analyzed by R package 'clusterProfiler', AgriGO2 (<http://systemsbiology.cau.edu.cn/agriGOv2/>) and REVIGO (<http://revigo.irb.hr/>).

Graphpad Prism 8.0.2 and Microsoft Excel 2016 were used for statistical analysis and graphs data presentation.

For manuscripts utilizing custom algorithms or software that are central to the research but not yet described in published literature, software must be made available to editors and reviewers. We strongly encourage code deposition in a community repository (e.g. GitHub). See the Nature Research [guidelines for submitting code & software](#) for further information.

Data

Policy information about [availability of data](#)

All manuscripts must include a [data availability statement](#). This statement should provide the following information, where applicable:

- Accession codes, unique identifiers, or web links for publicly available datasets
- A list of figures that have associated raw data
- A description of any restrictions on data availability

All data generated or analyzed during this study were included in this published article and supplementary files. Bio-reagents are available for research propose upon request from the corresponding author under a material transfer agreement.

Field-specific reporting

Please select the one below that is the best fit for your research. If you are not sure, read the appropriate sections before making your selection.

Life sciences Behavioural & social sciences Ecological, evolutionary & environmental sciences

For a reference copy of the document with all sections, see nature.com/documents/nr-reporting-summary-flat.pdf

Life sciences study design

All studies must disclose on these points even when the disclosure is negative.

Sample size	Sample sizes were determined by previous pilot experiments to be sufficient to achieve desired outcomes. Sample sizes are indicated in the Figures, legends and main text.
Data exclusions	No data were excluded from the analysis.
Replication	All experimental findings were reproduced in several independent biological experiments (n) with multiple technical replicates. The number of repeats is indicated in the figures and figure legends. Main Conclusions were confirmed in different plant genetic backgrounds and multiple temperature treatments. All attempts to replicate the experiments were successful and approved by multiple researchers.
Randomization	Samples of the same genotypes and growth conditions were randomly collected and pooled for downstream experiments.
Blinding	Investigators were not blinded to plant genotypes during experiments. The research materials are plants so the blinding design is not applicable to this system. Experiment results are not subjective.

Reporting for specific materials, systems and methods

We require information from authors about some types of materials, experimental systems and methods used in many studies. Here, indicate whether each material, system or method listed is relevant to your study. If you are not sure if a list item applies to your research, read the appropriate section before selecting a response.

Materials & experimental systems

n/a	Involved in the study
<input type="checkbox"/>	<input checked="" type="checkbox"/> Antibodies
<input checked="" type="checkbox"/>	<input type="checkbox"/> Eukaryotic cell lines
<input checked="" type="checkbox"/>	<input type="checkbox"/> Palaeontology and archaeology
<input checked="" type="checkbox"/>	<input type="checkbox"/> Animals and other organisms
<input checked="" type="checkbox"/>	<input type="checkbox"/> Human research participants
<input checked="" type="checkbox"/>	<input type="checkbox"/> Clinical data
<input checked="" type="checkbox"/>	<input type="checkbox"/> Dual use research of concern

Methods

n/a	Involved in the study
<input checked="" type="checkbox"/>	<input type="checkbox"/> CHIP-seq
<input checked="" type="checkbox"/>	<input type="checkbox"/> Flow cytometry
<input checked="" type="checkbox"/>	<input type="checkbox"/> MRI-based neuroimaging

Antibodies

Antibodies used

anti-HA antibody (Provided by Abcam, catalog number, ab137838, dilution 1:1,000);
 anti-Flag (Provided by ThermoFisher, catalog number, MA1-91878; dilution 1:1,000);
 anti-GFP antibody (Provided by ABClonal Biotechnology, catalog number AE012, dilution 1:1,000);
 anti-Tubulin antibody (Provided by Merck, catalog number 05-661; 1:2,000 dilution);
 anti-Mouse IgG, HRP-linked antibody (Provided by Cell Signaling, catalog number # 7076; 1: 5,000 dilution);
 anti-Rabbit IgG, HRP-linked antibody (Provided by Cell Signaling, catalog number # 7074; 1: 5,000 dilution);
 anti-DIG-AP (Provide by Roche, catalog number 11093274910; 1: 5,000 dilution).

Validation

1. The commercial anti-HA antibody has been validated for Immunoprecipitation and Western Blot in the several published papers

Validation

and used for co-immunoprecipitation in this study (Fig. 5e), and the antibody profile can be found in the following link: <https://www.abcam.com/ha-tag-antibody-ab137838.html>

2. The commercial anti-Flag antibody has been validated for Western Blot in the several published papers and used for co-immunoprecipitation in this study (Fig. 5e), and the antibody profile can be found in the following link: <https://www.thermofisher.com/antibody/product/DYKDDDDK-Tag-Antibody-clone-FG4R-Monoclonal/MA1-91878>

3. The commercial anti-GFP antibody has been well validated for Western Blot and Immunoprecipitation in the several published papers and in our manuscript (Figs. 5f and 7a, and Extended Data Fig.7d), and the antibody profile can be found in the following link: <https://abclonal.com/catalog-antibodies/MouseantiGFPtagmAb/AE012>

4. The commercial anti-Tubulin antibody has been well validated for Western Blot in the several published papers and used for loading control in our study (Extended Data Fig.7d), and the antibody profile can be found in the following link: https://www.merckmillipore.com/AU/en/product/Anti-Tubulin-Antibody-clone-AA2,MM_NF-05-661?ReferrerURL=https%3A%2F%2Fwww.google.com%2F&bd=1#overview

5. The commercial anti-Mouse IgG, HRP-linked antibody used for secondary antibody of Western blot has been validated n the several published papers, and the antibody profile can be found in the following link: <https://www.cellsignal.com/products/secondary-antibodies/%20anti-mouse-igg-hrp-linked-antibody/7076>

6. The commercial anti-Rabbit IgG, HRP-linked antibody used for secondary antibody of Western blot has been validated n the several published papers, and the antibody profile can be found in the following link: <https://www.cellsignal.com/products/secondary-antibodies/%20anti-rabbit-igg-hrp-linked-antibody/7074>

7.The commercial anti-Digoxigenin-AP, Fab fragments, has been well validated for In situ mRNA hybridisation in the several published papers and in our study (Figs.3b,d and 7e), and the antibody profile can be found in the following link: <https://www.sigmaldrich.com/catalog/product/roche/11093274910?lang=en®ion=AU>